https://doi.org/10.5194/bg-2021-40
Preprint. Discussion started: 1 March 2021

Biogeosciences Discussions

Cyanobacteria net community production in the Baltic Sea as inferred from profiling pCO_2 measurements

Jens Daniel Müller[1,2], Bernd Schneider[1], Ulf Gräwe[3], Peer Fietzek[4], Marcus Bo Wallin[5,6], Anna Rutgersson[5], Norbert Wasmund[7], Siegfried Krüger[3], and Gregor Rehder[1]

[1]Department of Marine Chemistry, Leibniz Institute for Baltic Sea Research Warnemünde, Rostock, Germany
[2]Environmental Physics, Institute of Biogeochemistry and Pollutant Dynamics, ETH Zurich, Zurich, Switzerland
[3]Department of Physical Oceanography and Instrumentation, Leibniz Institute for Baltic Sea Research Warnemünde, Rostock, Germany
[4]Kongsberg Maritime Germany GmbH, Hamburg, Germany
[5]Department of Earth Sciences, Uppsala University, Uppsala, Sweden
[6]Department of Aquatic Sciences and Assessment, Swedish University of Agricultural Sciences, Uppsala, Sweden
[7]Department of Biological Oceanography, Leibniz Institute for Baltic Sea Research Warnemünde, Rostock, Germany

Correspondence: Jens Daniel Müller (jensdaniel.mueller@usys.ethz.ch)

Abstract.

Organic matter production by cyanobacteria blooms is a major environmental concern for the Baltic Sea as it promotes the spread of anoxic zones. Partial pressure of carbon dioxide (pCO_2) measurements carried out on Ships of Opportunity (SOOP) since 2003 have proven to be a powerful tool to resolve the carbon dynamics of the blooms in space and time. However, SOOP measurements lack the possibility to directly constrain the depth–integrated net community production (NCP) due to their restriction to the sea surface. This study tackles the resulting knowledge gap through (1) providing a best–guess NCP estimate for an individual cyanobacteria bloom based on repeated profiling measurements of pCO_2 and (2) establishing an algorithm to accurately reconstruct depth–integrated NCP from surface pCO_2 observations in combination with modelled temperature profiles.

Goal (1) was achieved by deploying state–of–the–art sensor technology from a small–scale sailing vessel. The low–cost and flexible platform enabled observations covering an entire bloom event that occurred in July and August 2018 in the Eastern Gotland Sea. For the biogeochemical interpretation, recorded pCO_2 profiles were converted to C_T*, which is the dissolved inorganic carbon concentration normalised to alkalinity. We found that the investigated *Nodularia*–dominated bloom event had many biogeochemical characteristics in common with blooms in previous years. In particular, it lasted for about three weeks, caused a C_T* drawdown of 80 μmol kg^{-1}, and was accompanied by a sea surface temperature increase of 10 °C. The novel finding of this study is the vertical extension of the C_T* drawdown up to 12 m water depth. Integration of the C_T* drawdown across this depth and correction for vertical fluxes permit a best–guess NCP estimate of ~1.2 mol–C m^{-2}.

Addressing goal (2), we combined modelled hydrographical profiles with surface pCO_2 observations recorded by SOOP *Finnmaid* within the study area. Introducing the temperature penetration depth (TPD) as a new parameter to integrate SOOP observations across depth, we achieve a reconstructed NCP estimate that agrees to the best–guess within 10%.

https://doi.org/10.5194/bg-2021-40
Preprint. Discussion started: 1 March 2021


Biogeosciences Discussions Open Access EGU

Applying the TPD approach to almost two decades of surface pCO_2 observations available for the Baltic Sea bears the potential to provide new insights into the control and long–term trends of cyanobacteria NCP. This understanding is key for an effective design and monitoring of conservation measures aiming at a Good Environmental Status of the Baltic Sea.

1 Introduction

1.1 Net community production (NCP) in marine ecosystems

Net community production (NCP) of organic matter triggers many biogeochemical processes that control the functioning and state of marine ecosystems. Globally relevant examples are the biological carbon pump (Henson et al., 2011; Sanders et al., 2014) and the establishment of oxygen minimum zones (Gilly et al., 2013; Oschlies et al., 2018). In this biogeochemical context, we define NCP as the net amount of carbon fixed in organic matter (gross production minus respiration) that is produced in a defined water volume over a defined period. The reliable quantification of NCP is a prerequisite to understand subsequent biogeochemical transformation of the organic matter and its imprint on environmental conditions.

1.2 Baltic Sea

On a regional scale, NCP quantification is of particular importance to study the formation of anoxic conditions in stratified water bodies caused by the mineralisation of organic matter that was exported across a permanent pycnocline. This situation is typically encountered in semi–enclosed, silled estuaries such as the Baltic Sea. The deep basins of the Baltic Sea receive substantial amounts of oxygenated, salty water from the North Sea only during occasional major inflow events. Between inflow events, those water masses can stagnate for more than a decade below the permanent halocline (Mohrholz et al., 2015), which is located at around 60 m water depth in the Central Baltic Sea. The export of organic matter into the deep waters is the ultimate cause for the expansion of anoxic areas in the Baltic Sea, which are nowadays considered "the largest anthropogenically induced hypoxic areas in the world [a state which is] primarily linked to increased inputs of nutrients from land" (Carstensen et al., 2014). A quantitative and mechanistic understanding of near–surface organic matter production is key to understand, predict, and eventually counteract the expansion of those anoxic areas. The development of measures to reduce eutrophication and deep water anoxia represents a core component of the EU Marine Strategy Framework Directive (MSFD), which is implemented as the HELCOM Baltic Sea Action Plan (BSAP) and aims at a Good Environmental Status (GES).

1.3 Cyanobacteria blooms

The annual cycle of organic matter production in the Baltic Sea can be broadly divided into two events (Schneider and Müller, 2018). After a nitrate–fueled spring bloom, which is usually followed by a so-called blue water period with close–to–zero NCP rates, mid–summer cyanobacteria blooms develop in most years and cause a next pulse of NCP. The cyanobacteria blooms are limited to the months of June to August (Kownacka et al., 2020) and represent a common feature of the Baltic Sea ecosystem at least since the 1960s (Finni et al., 2001). The blooms are a major public concern, because they produce toxins and form

https://doi.org/10.5194/bg-2021-40
Preprint. Discussion started: 1 March 2021

thick surface scums lowering the recreational value of the Baltic Sea. From a biogeochemical perspective, the ability to fix nitrogen makes cyanobacteria independent from nitrate and aggravates the eutrophication state of the Baltic Sea. Whether their growth is limited by the availability of phosphate remains an ongoing debate (Nausch et al., 2012), although the highly variable C:P ratio of their biomass (Nausch et al., 2009) indicates phenotypic plasticity. Other ongoing debates in the field of cyanobacteria research address the fate of the produced organic matter and its transfer into the food web (Karlson et al., 2015), the intensification of cyanobacteria blooms through positive feedback loops between organic matter production, deep water anoxia and the release of phosphate from anoxic sediments (Vahtera et al., 2007), as well as their response to ongoing changes in salinity, temperature and the partial pressure of carbon dioxide (pCO_2) (Olofsson et al., 2019, 2020). The limited understanding of the factors that control the blooms hinders the reliable prediction of the future state of the Baltic Sea and therefore the prioritisation of conservation measures (Elmgren, 2001). In particular, it remains challenging to disentangle how expected trends – including warming, reduced nutrient loads, and increasing pCO_2 – might impact cyanobacteria growth (Meier et al., 2019; Saraiva et al., 2019).

1.4 Quantification of NCP

Striving for a better understanding of the ecosystem impact of cyanobacteria blooms, the accurate quantification of produced organic matter is key. In this regard, NCP could in principle be quantified directly as an increase in particulate organic carbon (POC). However, POC measurements would not detect the amount of organic matter that was exported between observations (Wasmund et al., 2005) and also fail to achieve the required spatio–temporal resolution due to a low degree of automation. As an alternative, it is possible to quantify NCP through the drawdown of dissolved inorganic carbon (C_T) from the water column (Schneider et al., 2003). From a biogeochemical perspective, the determination of NCP in terms of carbon is ideal, because carbon is the major component of organic matter and directly related the amount of oxygen (O_2) that is consumed during mineralisation. In principle, NCP could as well be estimated from O_2 time series. However, the equilibrium reactions of carbon dioxide (CO_2) in seawater result in higher re–equilibration times of CO_2 with the atmosphere compared to O_2, which results in substantially longer signal preservation and makes C_T the preferred tracer for NCP. During the Baltic Sea spring bloom, the tracing of nutrient consumption is a meaningful alternative to quantify NCP and convincingly leads to comparable results to the C_T approach (Wasmund et al., 2005). However, nutrient time series do not allow for determining cyanobacteria NCP due to the organism's ability to fix nitrogen and their highly variable C:P ratios. In conclusion, the well established C_T approach is the favorable method to determine cyanobacteria NCP. However, it should be noted that NCP estimates derived from this approach include the formation of POC and dissolved organic carbon (DOC). The produced DOC contributes ~20% to POC (Hansell and Carlson, 1998; Schneider and Kuss, 2004) and is not likely to be vertically exported.

1.5 Previous studies

Among previous attempts to trace and quantify the organic matter production of cyanobacteria blooms, automated measurements of the partial pressure of carbon dioxide (pCO_2) on the Ship of Opportunity (SOOP) *Finnmaid* played a pivotal role. Those measurements were started in 2003 and it was demonstrated that highly accurate time series of changes (not absolute

https://doi.org/10.5194/bg-2021-40
Preprint. Discussion started: 1 March 2021

values) in C_T can be derived from pCO_2 observations (Schneider et al., 2006). The conversion from pCO_2 to C_T relies on a fixed alkalinity (A_T) estimate and is applicable under the condition that internal sources of A_T can be excluded, which is the case in the Baltic Sea due to the absence of calcifying plankton (Tyrrell et al., 2008). The derived parameter is comparable to directly measured C_T normalised to A_T, and in the following referred to as C_T*. For several years of SOOP observations, it was shown that the C_T* drawdown during mid–summer cyanobacteria blooms occurs in pulses of days to weeks, primarily during calm, sunny days. Further, it was found that the C_T* drawdown correlates well with the co–occurring increase in sea surface temperature (SST), rather than with absolute SST. This relationship was attributed to a common driver, which is the light dose received by the water mass under consideration (Schneider and Müller, 2018).

Despite the successful investigation of cyanobacteria blooms through SOOP pCO_2 observations, providing a depth–integrated estimate of NCP in units of moles carbon fixed per surface area remains challenging due to the restriction of SOOP observations to surface waters. Previous studies aiming at a depth–integrated NCP estimate either simply assumed that the C_T drawdown reached as far down as the water inlet of the measurement system (Schneider and Müller, 2018) or relied on a modelled mixed layer depth for the integration of surface observations across depth (Schneider et al., 2014). However, in the absence of any vertically resolved measurements, neither approach could be validated. Likewise, remote sensing approaches resolve the spatial coverage of the blooms (Hansson and Hakansson, 2007; Kahru and Elmgren, 2014), but fail to detect their vertical extent (Kutser et al., 2008) and quantify NCP. Finally, regular research vessel cruises allow for the determination of a full suite of biogeochemical parameters from discrete water samples and even the experimental determination of carbon fixation rates through ^{14}C incubations (Wasmund et al., 2001, 2005). Incubation experiments can provide valuable information about instantaneous rates of NCP, but – in contrast to time series observations such as obtained by SOOP measurements – do not allow to integrate observed changes over time and constrain budgets of biogeochemical transformations. This integration over time requires several weeks of repeated observations to resolve the progression of entire bloom events, ideally covering a station network to average bloom patchiness.

1.6 This study

This study builds upon the previous success to determine NCP based on pCO_2 time series, but extends the approach to vertically resolved observations for the first time. The primary goals of this study are to

(1) provide a best–guess estimate for the depth–integrated NCP of an individual cyanobacteria bloom based on the full suite of depth–resolved in situ measurements and

(2) establish an algorithm to reconstruct depth–integrated NCP based on surface pCO_2 observations and modelled hydrographical profiles

Achieving goal (2) and applying the algorithm to almost two decades of SOOP pCO_2 observations in the Baltic Sea would not only allow to determine long-term trends of cyanobacteria NCP, but also enable disentangling its drivers through a comparison of NCP across years characterized by different environmental conditions such as SST, pCO_2 and nutrient availability.

https://doi.org/10.5194/bg-2021-40
Preprint. Discussion started: 1 March 2021

2 Methods

2.1 Overview

Profiling in situ sensor measurements and water sampling were performed on board the 27ft sailing vessel SV *Tina V* in the framework of the field sampling campaign "BloomSail". The study area was located in the Central Baltic Sea and extended about 25 nautical miles from the coast of Gotland into the Eastern Gotland Basin (Fig. 1). Measurements were performed during eight cruises covering the period July 6 to August 16, 2018 (Fig. 2).

A custom–made sensor package configured at IOW's Innovative Instrumentation department was deployed to perform pCO_2 and conductivity, temperature and depth (CTD) measurements. The sensor package was either towed near the water surface while cruising or lowered to at least 25 m water depth at designated profiling stations. This study focuses exclusively on the vertical profiles recorded at stations 02 – 12 (Fig. 1b), whereas profiles in coastal regions with water depths below 60 m and towed surface measurements were not taken into account. In addition to the sensor measurements, discrete samples for dissolved inorganic carbon (C_T), total alkalinity (A_T) and phytoplankton counts were collected. Track coordinates were continuously recorded with a tablet computer (Galaxy Tab Active, Samsung Electronics, Suwon, South Korea).

In addition to the field sampling campaign, atmospheric measurements of wind speed and pCO_2 were provided by an ICOS (Integrated Carbon Observation System) station permanently operated on the island Östergarnsholm (Fig. 1B). Furthermore, sea surface pCO_2 and temperature (SST) were also determined on the SOOP *Finnmaid*, regularly crossing the field study area (Fig. 1B). High–resolution hydrographical model data were obtained from the Generalized Estuarine Turbulence Model (GETM) along a vertical section following the *Finnmaid* track.

2.2 Field sampling campaign

2.2.1 CTD measurements

CTD measurements were performed with a SBE 16 SEACAT instrument (serial number 2557; Sea-Bird Electronics, Bellevue, USA). Temperature and salinity sensors were pre–calibrated at IOW's sensor calibration laboratory. The manual operation of the sensor package was guided by real–time display of data submitted through a strain–relieved cable. Data stored on an internal memory were used for analysis. The CTD logging frequency was 15 seconds and observations were linearly interpolated to match the higher measurement frequency of the pCO_2 sensor (for additional details see Appendix A2). The CTD instrument supplied auxiliary sensors with power and served as a central unit to record and transmit analogue output signals.

2.2.2 pCO_2 sensor measurements

The submersible CO_2 sensor used in this study, a CONTROS HydroC® CO_2 (formerly Kongsberg Maritime Contros, Kiel, Germany; now -4H-JENA engineering, Jena, Germany), uses membrane equilibration of a headspace and subsequent optical Non–Dispersive Infra–Red (NDIR) absorption to determine the pCO_2 in water (Fietzek et al., 2014).

https://doi.org/10.5194/bg-2021-40
Preprint. Discussion started: 1 March 2021

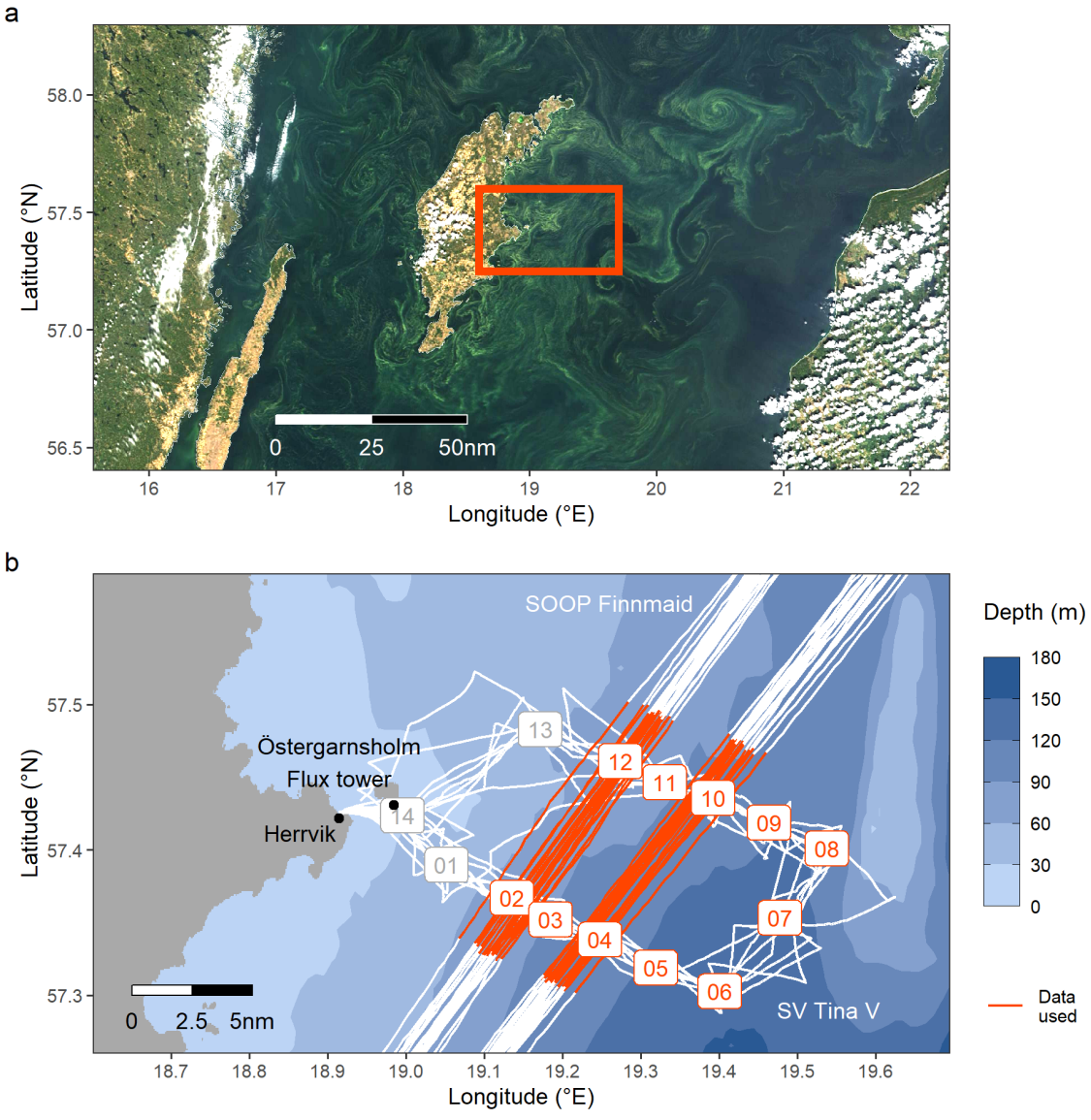

Figure 1. (a) Extent of the cyanobacteria bloom on July 26, detectable as greenish patterns in a true color satellite image (MODIS Aqua/Terra, Nasa Worldview) showing the Central Baltic Sea around the island of Gotland. The box indicates the study area as shown in (b), a bathymetric map with the cruise tracks of SV *Tina V* (BloomSail campaign) and SOOP *Finnmaid*. BloomSail stations and the SOOP sub–transects used in this study are highlighted in red. The ICOS flux tower for atmospheric measurements is located on the island of Östergarnsholm.

https://doi.org/10.5194/bg-2021-40
Preprint. Discussion started: 1 March 2021

Biogeosciences Discussions Open Access EGU

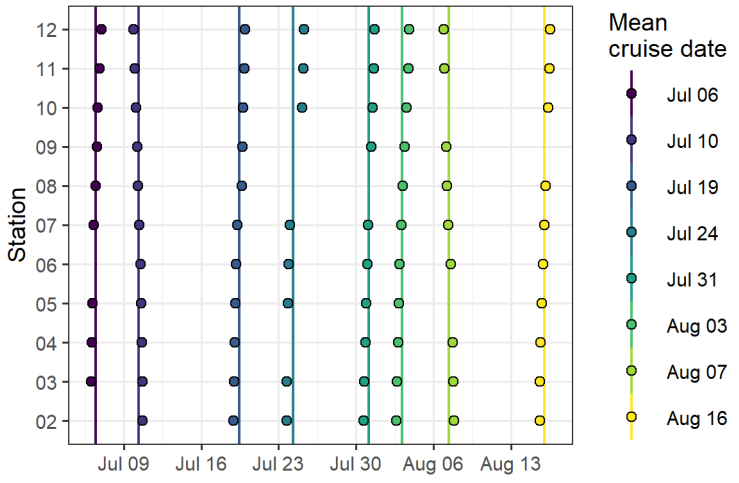

Figure 2. Overview on profiling sensor measurements performed at stations 02 – 12 (Fig. 1). Individual sampling events are displayed as points, whereas vertical lines indicate the mean date of each cruise event.

A pre– and post–deployment calibration of the sensor was performed by the manufacturer. pCO_2 data were post–processed taking into account the pre– and post–deployment calibration polynomials, as well as zeroing signals regularly recorded during each deployment. The post–processing resulted in an accuracy of 1% of reading (Fietzek et al., 2014). For details concerning sensor calibration, configuration, and signal post–processing, see Appendices A1 – A3.

Although the pCO_2 sensor achieves low and reproducible response times through active pumping of water onto the membrane, a correction of the response time (τ) was applied following Bittig et al. (2018). After the response time correction, the mean absolute pCO_2 difference between the up– and downcast profile was <2.5 μatm in the upper 5 m of the water column and <7.5 μatm across the upper 20 m (Fig. A2). For details concerning the response time correction, see Appendix A4.

The biogeochemical interpretation of the pCO_2 data was based on downcast profiles only. Since downcasts were started after complete equilibration of the pCO_2 sensor in near–surface waters, the applied response time correction has only a minor impact on the derived NCP estimate.

2.2.3 Discrete C_T, A_T and phytoplankton sampling

Discrete samples were collected at stations 07 and 10 (Fig. 1B) with a manually released Niskin bottle. The sampling depth was estimated based on the released line. C_T and A_T samples were filled into 250 ml SCHOTT–DURAN bottles and poisoned with 200 μL saturated HgCl solution within 24 hours after sampling. Samples were stored dark and cool, transported to IOW, and analysed in the laboratory within no more than 21 days after sampling. C_T was determined with an Automated Infra Red Inorganic Carbon Analyzer (AIRICA, MARIANDA, Kiel, Germany) and A_T was analysed by open cell titration (Dickson et al., 2007). C_T and A_T measurements were referenced to certified reference materials from batch 173 (Dickson et al., 2003). Phytoplankton samples were fixed with Lugol solution, and community composition and biomass were determined by

https://doi.org/10.5194/bg-2021-40
Preprint. Discussion started: 1 March 2021

microscopic counts according to the Utermöhl method (HELCOM, 2017). For details on the analysis of discrete samples, see Appendix B.

2.3 Atmospheric measurements

Meteorological observations were provided by the ICOS flux tower (Fig. 1b) located on the southernmost tip of the Island of Östergarnsholm (57.43010 °N, 18.98415 °E; Rutgersson et al., 2020). Atmospheric pCO_2 was recorded with an atmospheric profile system (AP200, Campbell Scientific, Logan, USA) mounted with a CO_2/H_2O gas analyzer (LI-840A, LI-COR Biosciences, Lincoln, USA). Wind speed was measured with a wind monitor (Young, Michigan, USA) at 12 m above mean sea level. Wind speed and pCO_2 data were averaged over 30 min intervals for further analysis. Measured wind speed was converted to U_{10}, the wind speed at 10 m above sea level (Winslow et al., 2016), to be consistent with the gas exchange parameterisation (see Sect. 2.4.3).

2.4 NCP best–guess estimate

The determination of NCP in this study relies on the interpretation of observed temporal changes in the dissolved inorganic carbon concentration (C_T*) across the water column. We refer to this estimate as our best–guess, as it is well-constrained by high-quality measurements and therefore as close to the truth as currently possible. Conceptually, our calculations follow the idea of a one–dimensional box model approach, which does not resolve regional variability within the research area, i.e. it neglects lateral water mass transport. With this approach it is possible to calculate NCP from the observed changes in C_T* (Sect. 2.4.1) after vertical gridding and regional averaging of the profiles (Sect. 2.4.2) and applying corrections for CO_2 fluxes caused by air–sea gas exchange (Sect. 2.4.3) and vertical mixing (Sect. 2.4.4).

2.4.1 C_T* calculation

C_T* was calculated from the measured profiles of temperature and response time corrected pCO_2 (Schneider et al., 2014), as well as the mean A_T (1720 μmol kg^{-1}) and mean salinity (6.9) determined from discrete samples collected across the upper 20 m of the water column and the entire observation period (Fig. B1). Calculations were performed with the R package seacarb (Gattuso et al., 2020), using the CO_2 dissociation constants for estuarine waters from Millero (2010).

The calculated C_T* represents an alkalinity– and salinity–normalised estimate of the dissolved inorganic carbon concentration. C_T* is suitable to accurately determine changes rather than absolute values of the dissolved inorganic carbon concentration and therefore the preferred variable to quantify NCP. The uncertainty in the determination of changes of C_T* is below 2 μmol kg^{-1} when the mean A_T is constrained within $\pm$30 μmol kg^{-1} (see Appendix C1 for a detailed assessment).

2.4.2 Vertical gridding and regional averaging

The regional averaging of observations across the study area and the calculation of temporal changes at individual depth levels required a vertical gridding of the profiling sensor measurements. The vertical gridding of individual profiles was achieved

https://doi.org/10.5194/bg-2021-40
Preprint. Discussion started: 1 March 2021

by calculating mean values within 1 m depth intervals. Downcast profiles with missing observations from two or more depth intervals caused by zeroing measurements of the pCO_2 sensor were discarded, which affected 8 out of 86 recorded profiles. For each of eight cruise events (Fig. 2), regionally averaged profiles were further calculated as mean values within each depth interval across all stations. Based on those mean, vertically gridded cruise profiles, incremental and cumulative changes over time were calculated for each depth interval. Throughout the manuscript, observations averaged across the upper 0 – 6 m of the water column are referred to as surface observations.

2.4.3 Air–sea CO_2 flux

The air–sea gas exchange of CO_2 (F) was calculated from sea surface pCO_2, salinity and temperature, in combination with atmospheric pCO_2 and wind speed (U_{10}) according to Wanninkhof (2014). For the calculation, sea surface observations were linearly interpolated to match the temporal resolution of atmospheric measurements.

2.4.4 Vertical entrainment flux of CO_2 through mixing

Due to the stable thermocline present between June 6 and August 7, vertical mixing of C_T* across the 12 m integration depth layer was neglected during this period. However, clear signals for significant vertical entrainment of C_T* across this layer were recorded between August 7 and 16. This entrainment was quantified assuming an instantaneous complete vertical mixing to 17 m water depth after August 7. For this simplified scenario, the C_T* flux across the 12 m depth layer was estimated based on a mass–balance of C_T*, which behaves conservatively with respect to mixing (see Appendix C2 for details).

2.5 NCP reconstruction from surface pCO_2 observations and hydrographical profiles

Calculating depth–integrated NCP from a time series of surface pCO_2 observations, such as provided by SOOP lines, also relies on the conversion of pCO_2 to C_T*. Furthermore, the change of C_T* over time in the surface water needs to be multiplied with an integration depth estimate to derive an inventory change. Here, we tested two approximations of this integration depth, which are:

- Mixed layer depth (MLD)
- Temperature penetration depth (TPD)

MLD and TPD are described in detail in Sect. 2.5.3. The two parameterisations were further applied to following two test data sets, both of which contain the required surface pCO_2 and vertically resolved temperature and salinity data:

- In situ data from the BloomSail campaign without pCO_2 data at depth (SV Tina V (surface only))
- Combined SOOP surface pCO_2 observations and modelled salinity and temperature profiles (SOOP Finnmaid + GETM model)

The derived four reconstructed NCP time series were compared to the best–guess estimate (i.e. the estimate based on the vertically resolved pCO_2 observations from this study).

https://doi.org/10.5194/bg-2021-40
Preprint. Discussion started: 1 March 2021

2.5.1 SOOP *Finnmaid* surface pCO_2

SOOP *Finnmaid* regularly commutes between Helsinki in Finnland and Travemünde in Germany thereby crossing the entire Central Baltic Sea and our study area on the east coast of Gotland every 1 – 2 days. On board SOOP *Finnmaid*, pCO_2 is measured with a bubble–type equilibrator system supplied with water from an inlet at around 3 m water depth. Details of the measurement set–up are described in Schneider et al. (2014) and data are submitted on a regular basis to the Surface Ocean CO_2 Atlas SOCAT (Bakker et al., 2016). The primary measurement system used to determine pCO_2 in this study is a NDIR sensor (LI-6262, LI-COR Biosciences, Lincoln, USA). The ferrybox unit is also equipped with an additional methane/carbon dioxide analyzer (Greenhouse Gas Analyzer DLT 100, type 908-0011, Los Gatos Research, San Jose, USA), providing independent pCO_2 observations (Gülzow et al., 2011). Intercomparison of both systems is routinely used to ensure the correct functioning of the instrumentation. In this study, a data gap caused by malfunctioning of the primary LI-COR system was filled by including data recorded with the Los Gatos system on six cruises between July 8 and 16 (see Appendix D for details). The mean regional pCO_2, sea surface temperature (SST) and salinity (SSS) were calculated for each crossing of the study area (Fig. 1B). Based on those mean values, C_T* was calculated following the procedure outlined in Sect. 2.4.1. A remaining gap in the SOOP time series was filled with two in situ C_T* observations from the BloomSail campaign (July 19 and 24).

2.5.2 GETM model temperature and salinity

Surface SOOP measurements were complemented with the vertical distribution of salinity and temperature from the output of a numerical ocean model of the Baltic Sea. The deployed General Estuarine Turbulence Model (GETM) has a horizontal resolution of 1 nautical mile and 50 vertical terrain–following levels. The uppermost level has a thickness of maximum 50 cm to properly represent SST and ocean–atmosphere fluxes. The computation of the atmospheric fluxes is based on the parameterisation of Kara et al. (2005). The model run covers the period 1961 – 2019. A detailed analysis of the ocean model performance is given in Placke et al. (2018) and Gräwe et al. (2019). For the present study, we used a model run restarted in 2003 with the atmospheric forcing from the operational reanalysis data set of the German weather service (Zängl et al., 2015). Additionally, we implemented the Langmuir–circulation parameterisation of Axell (2002), to account for wind–wave induced variation in the mixed layer depth. Model results were averaged over 24 h and interpolated to a standardised section with 2 km horizontal and 1 m vertical resolution, which follows the mean *Finnmaid* cruise track. Based on this standard section, daily mean profiles within the study area were computed and linearly interpolated to match the exact times of *Finnmaid* crossings.

2.5.3 Parameterisation of the integration depth

In this study, two parameters were used to integrate surface observations across depth, namely the classical mixed layer depth (MLD) and the newly introduced temperature penetration depth (TPD).

MLD was defined as the shallowest depth at which seawater density exceeds the density at the surface by more than 0.1 kg m^{-3} (Roquet et al., 2015). According to this definition, MLD characterises the thermohaline structure of the water column and often (but not necessarily) approximates the depth to which surfaces water masses are actively mixed. The defini-

https://doi.org/10.5194/bg-2021-40
Preprint. Discussion started: 1 March 2021

tion through a fixed density threshold further implies that gradual changes of temperature with depth are not reflected by this parameter.

TPD was defined as the SST increase divided by the integrated warming signal across the water column (i.e. the sum of all positive temperature changes within 1m depth intervals) that occurred between two sampling events (for illustration see Fig. C4A). TPD is only applicable when SST increases and has units of metres. According to its definition, TPD characterises the mean penetration depth of a warming signal and takes gradual changes of temperature across depth into account. To illustrate the TPD concept, it should be noted that a homogeneous warming signal that ceases abruptly at 10 m water depth would result in the same TPD as a warming signal that decreases linearly from the surface to 20 m water depth (TPD is 10 m in both cases). The TPD approach is motivated by the assumption that primary production and temperature increase are both primarily controlled by the light dose that a water parcel received (Schneider et al., 2014) and therefore show similar patterns.

Based on MLD or TPD, vertically integrated changes of C_T* were reconstructed as the product of incremental changes of surface C_T* between cruise days and one of the two integration depth estimates. The reconstructed integrated changes of C_T* were further corrected for air–sea fluxes of CO_2 according to section 2.4.3. Please note that neither the MLD nor the TPD approach allows to resolve vertical entrainment fluxes, because profiles of C_T* are not reconstructed (compare section 2.4.4). In analogy to TPD, the penetration depth of C_T* drawdown (CPD) was defined as the decrease of C_T* at the surface divided by the integrated loss of C_T* across the water column (Fig. C4B).

3 Results

3.1 Dynamics of temperature, pCO_2, C_T* and phytoplankton biomass

Between July 6 and August 16, a total number of 78 complete vertical CTD and pCO_2 downcast profiles were recorded (Fig. 2 and 3). C_T* was calculated and profiles were regionally averaged for each of the eight cruise events (Fig. 4). Since the first cruise of the BloomSail expedition on July 6, sea surface temperature (SST) increased steadily from ~15 °C to peak values of 25 °C (Fig. 4 and 5) observed on August 3. Sea surface pCO_2 was already as low as ~100 μatm at the beginning of July (Fig. 5a) and decreased further to the lowest values of ~70 μatm on July 24. The drop in pCO_2 and the simultaneous increase in SST correspond to a decrease of C_T* of almost 90 μmol kg^{-1} (Fig. 4). During this period of intense primary production, the regional variability of SST, pCO_2, and C_T* across stations was low compared to their temporal change (Fig. 5a–b; Fig. C3). The regional variability is slightly higher when including the coastal stations 01, 13, and 14 (results not shown), but is generally lower than suggested by the bloom patchiness typically observed through remote sensing (Fig. 1a). With respect to pCO_2 dynamics, it should be noted that (i) the observed temperature increase and C_T* drawdown have opposing effects on pCO_2 and (ii) the change of pCO_2 per change in C_T* is generally low at low absolute pCO_2. The observed C_T* dynamics in surface waters are clearly attributable to the primary production activity of phytoplankton and go along with an observed increase of the biomass of *Nodularia* sp. (Fig. B2), which also peaked on July 24.

Between the extremes of pCO_2 and C_T* (minimum on July 24) and SST (maximum on August 3), a noticeable increase of surface C_T* was observed on July 31, which was accompanied by a higher regional variability across the station network

https://doi.org/10.5194/bg-2021-40
Preprint. Discussion started: 1 March 2021

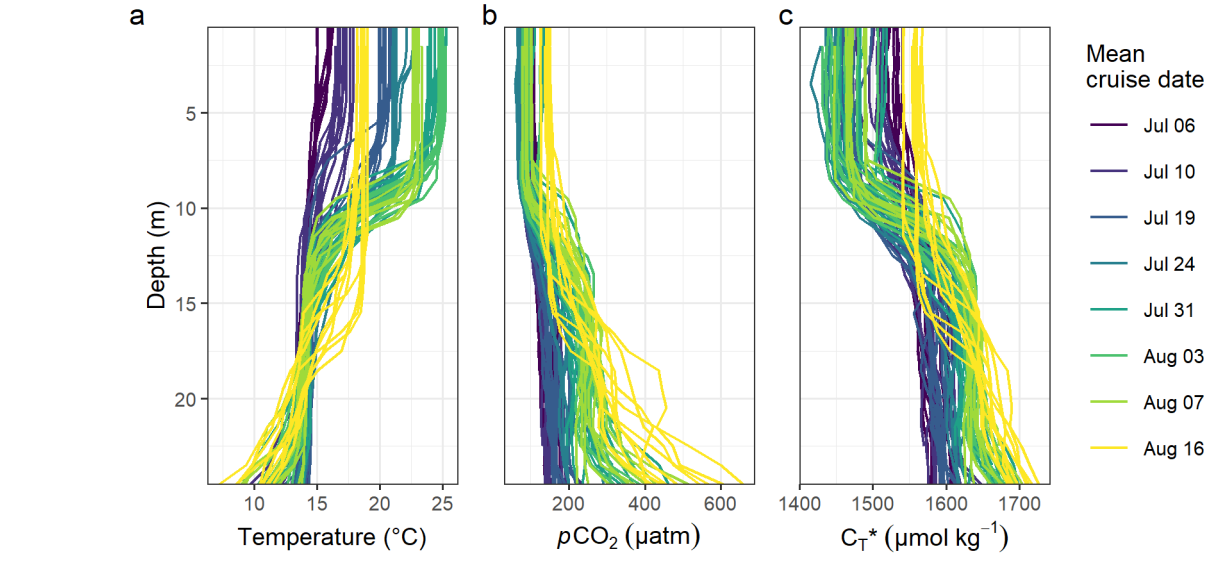

Figure 3. Overview of (a) temperature, (b) pCO_2 and (c) C_T* profiles recorded throughout the BloomSail field sampling campaign on board SV *Tina V*.

(Fig. 5a,c). The temporary C_T* increase was limited to the north–eastern stations 07 – 10 (Fig. C3) and paralleled by a drop in salinity and elevated A_T at the same stations (Fig. B1). It is therefore attributable to the lateral exchange of water masses. All signals of this lateral intrusion vanished within a week. At the other stations (02 – 06 and 11 – 12), no noticeable signs of water mass exchange or C_T* changes were observed between July 24 and August 3, indicating that NCP had ceased during this period. During the first two weeks of August the study area was affected by increased wind speeds, causing a decrease of SST back to ~18 °C. The simultaneous return of surface pCO_2 to ~150 μatm corresponded to a C_T* increase of ~100 μmol kg^{-1}.

The observed surface warming and C_T* drawdown extended vertically to a water depth of ~10 m (Fig. 4). On the first cruise day (July 6), the vertical distribution of C_T* and temperature was still relatively homogenous. C_T* at 25 m water depth was ~70 μmol kg^{-1} higher than at the surface. Likewise, the temperature gradient covered only ~3 °C from 16 °C at the surface to 13 °C at depth. The warming of surface waters caused an increasingly stable thermocline to be established at around 10 m water depth, reaching a temperature gradient of ~10 °C across 5 m on August 3. Continuous and uniform consumption of C_T* within the surface layer enhanced the vertical C_T* gradient to >150 μmol kg^{-1} between the surface and 25 m water depth. The C_T* drawdown was observed to a maximum depth of 12 m.

Between August 7 and 16 the SST drop of ~6°C was accompanied by a temperature increase in deeper water layers (11 – 17 m) of up to 5 °C. This vertical redistribution of heat indicates vertical mixing of water masses, which was also reflected in a steep increase of C_T* in the surface water and a loss of C_T* between 11 – 17 m (Fig. 3 and 4).

https://doi.org/10.5194/bg-2021-40
Preprint. Discussion started: 1 March 2021

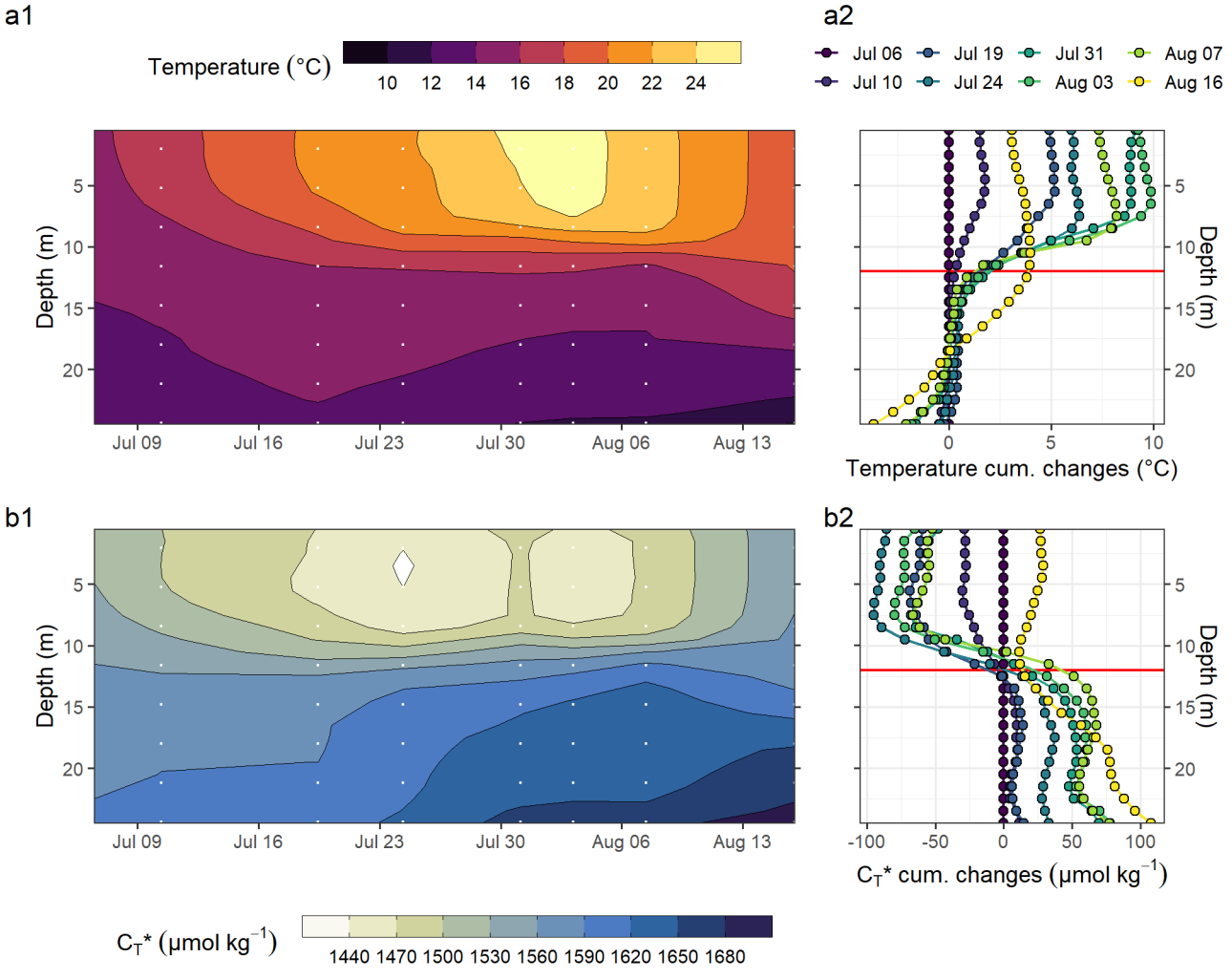

Figure 4. (a) Temperature and (b) C_T* between July 6 and August 16 displayed as (1) Hovmoeller plots and (2) profiles of cumulative changes since the first cruise on July 6. Mean cruise dates are indicated by white dots in (1) and the integration depth of 12 m is indicated as a red, horizontal line in (2).

3.2 NCP best–guess based on profiling measurements

Net community production (NCP) was determined through vertical integration of the observed consumption of C_T* from the surface to a water depth of 12 m. The chosen integration depth reflects the maximum penetration depth of the incremental (i.e. between cruise days), as well as the cumulative (i.e. from July 6 – 24) C_T* drawdown (Fig. 4). Likewise, about 95% of the
310 cumulative warming signal, which refers to positive temperature changes integrated over depth, occurred above 12 m.

https://doi.org/10.5194/bg-2021-40
Preprint. Discussion started: 1 March 2021

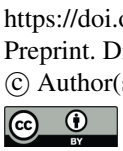

Biogeosciences
Discussions
Open Access
EGU

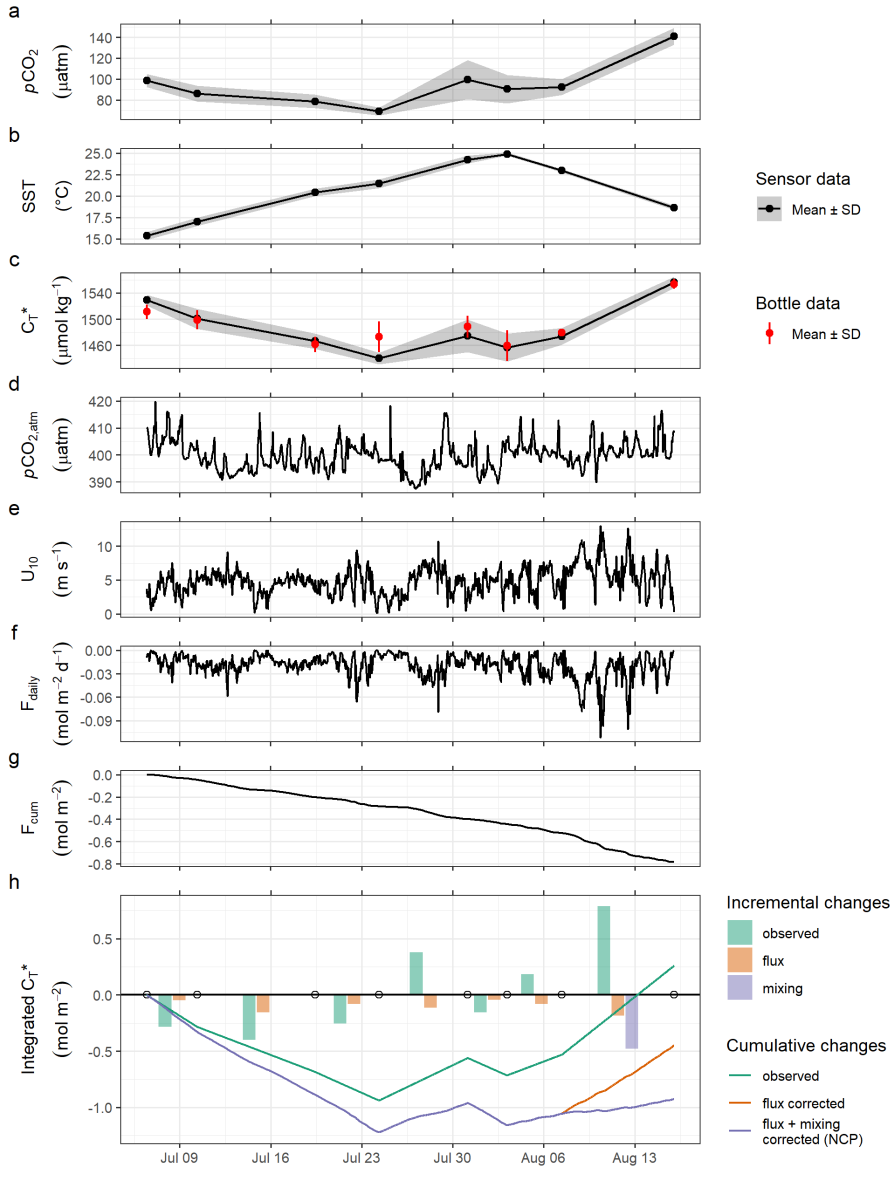

Figure 5. Time series displaying from top to bottom: Surface water observation of (a) pCO_2, (b) temperature, (c) C_T* with grey ribbons indicating the standard deviation across stations; atmospheric observations of (d) $pCO_{2,atm}$, (e) wind speed at 10 m, (f) daily and (g) cumulative air–sea fluxes of CO_2; as well as (h) the derived water column inventory changes of C_T*. In (h), bars represent incremental changes between cruise events (open circles), whereas lines represent cumulative changes since the first cruise. Colours distinguish observed C_T* changes from values referring to the applied air–sea CO_2 flux and mixing correction. Net community production (NCP) is equal to the flux and mixing corrected cumulative changes of C_T* (purple line) and reaches its peak value on July 24.

https://doi.org/10.5194/bg-2021-40
Preprint. Discussion started: 1 March 2021

Until July 24, the depth–integrated C_T* consumption amounted to ~0.9 mol m^{-2} (Fig. 5H). This observed C_T* consumption was corrected for air–sea fluxes of CO_2 (F). Between July 6 and August 7, the cumulative flux (F_{cum}) amounted to around -0.5 mol m^{-2} (Fig. 5G), with a negative sign representing CO_2 uptake from the atmosphere. In the absence of noticeable vertical mixing, this flux was entirely added to the observed C_T* consumption. Only between August 7 and 16, when mixing to about 17 m water depth was observed, a significant fraction of the CO_2 taken up from the atmosphere was transported below 12 m water depth. To account for the partial loss of airborne CO_2 to deeper waters during this 9 day–period, only 12/17 of F_{cum} during this time (-0.2 mol m^{-2}), which is the fraction that would remain in the upper water column, was added to the observed C_T* consumption. In addition, a significant amount of C_T* entrainment (~0.5 mol m^{-2}) into the surface layer was caused by the vertical mixing between August 7 and 16 (Fig. 5H and C2).

After correction for air–sea fluxes and vertical entrainment of CO_2, the cumulative changes of depth–integrated C_T* represent the NCP between 0 – 12 m water depth (Fig. 5H). The peak NCP value of ~1.2 mol m^{-2} was observed on July 24 and is of primary interest because it reflects the amount of organic matter that was produced and is potentially available to be either exported or remineralised. After July 24, no signs of continued NCP were observed. Accordingly, the following attempt to reconstruct NCP based on surface pCO_2 observations focuses on the period July 6 – 24.

3.3 NCP reconstruction based on surface pCO_2 and hydrographical profiles

The reconstruction of depth–integrated NCP was tested for two data sets containing the same type of information, namely the observed changes in surface pCO_2 and vertical profiles of seawater salinity and temperature. The first data set "SV Tina V (surface only)" contains the surface pCO_2 data recorded during the BloomSail expedition, as well as the complete CTD profiles. The second data set ("SOOP Finnmaid + GETM model") combines surface pCO_2 observations from SOOP *Finnmaid* with seawater salinity and temperature as estimated with the GETM model. For both data sets C_T* time series were calculated based on the same mean A_T.

An almost identical decrease of surface C_T* of ~50 μmol kg^{-1} was determined between July 6 and 16 (Fig. 6A), based on the completely independent pCO_2 data recorded on SOOP *Finnmaid* and SV *Tina V*. Likewise, a very similar increase in C_T* between August 6 and 15 was determined from both independent observational data sets. The good agreement between the independent observations justifies that a data gap due to failure of instrumentation on the SOOP was filled with two observations from SV *Tina V* on July 19 and 24 (open circles in (Fig. 6A).

Good agreement was also found for the spatio–temporal dynamics of observed and modelled seawater temperature (Fig. 6B). Observed and modelled SST agreed within 1 °C over the entire observation period, despite an absolute change spanning almost 10 °C. Slightly higher deviations between observed and modelled temperature were found around the thermocline, where the observational record revealed a stronger temperature gradient. This difference is likely due to an imperfect representation of Langmuir circulation in the model (Axell, 2002), whereas the absence of increased light attenuation caused by phytoplankton particles was previously found to have only minor impacts on modeled SST dynamics (Löptien and Meier, 2011). Most importantly, the mean temperature penetration depths (TPD) derived from the observational and model data differ less than 1 m, indicating that surface warming and the integrated heat uptake are accurately represented by the model. The TPD (mean

https://doi.org/10.5194/bg-2021-40
Preprint. Discussion started: 1 March 2021

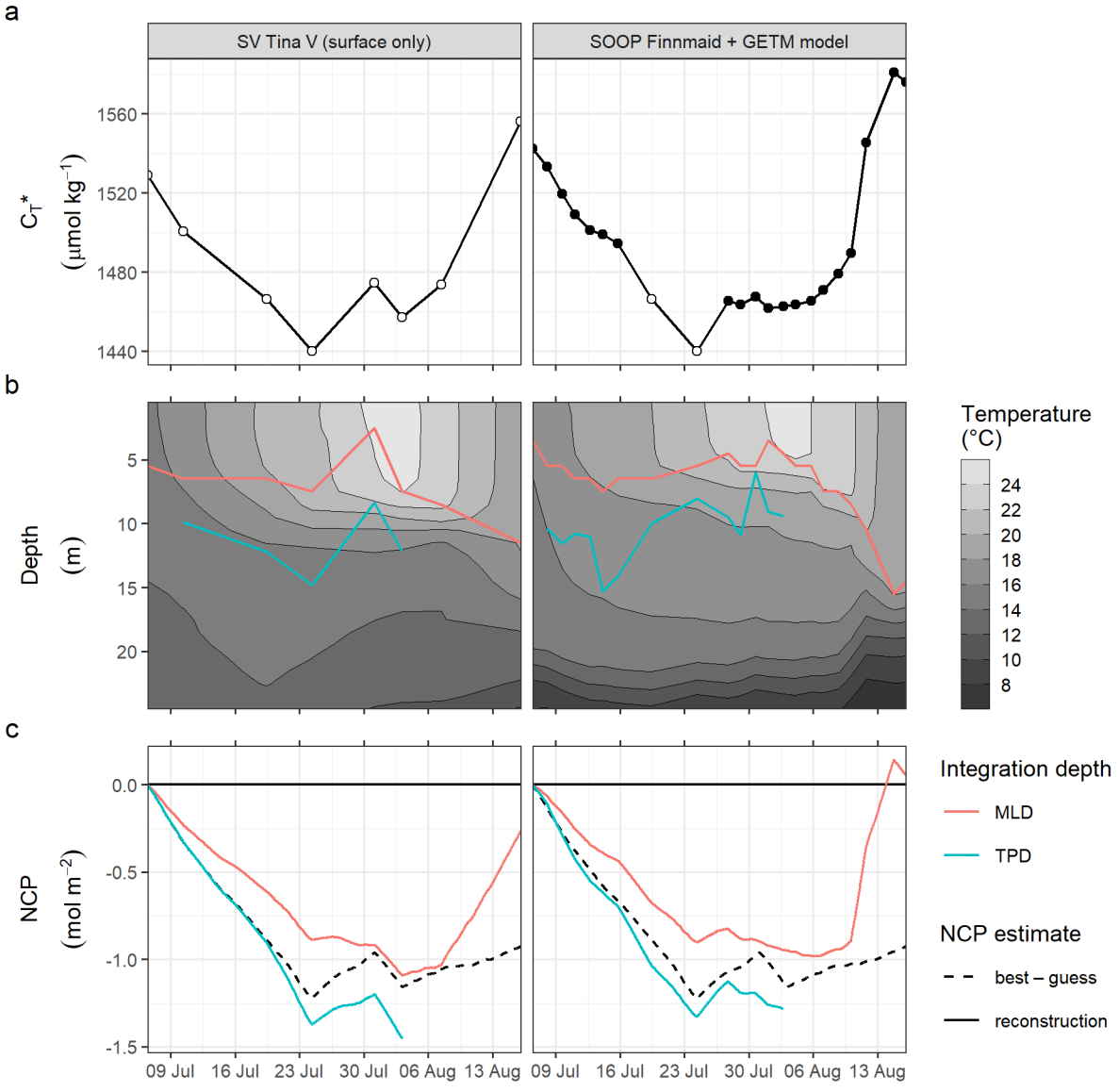

Figure 6. Time series illustrating the reconstruction of depth–integrated NCP from surface C_T* and vertically resolved hydrographical parameters. Displayed are results based on two test data sets, namely observations from SV *Tina V* without C_T* data at depth (left panels) and a combination of SOOP C_T* and modelled hydrographical data (right panels). From top to bottom, panels represent (a) surface C_T*, (b) the vertical distribution of temperature together with the mixed layer depth (MLD) and temperature penetration depth (TPD) for each cruise day, and (c) depth–integrated NCP comparing the reconstruction approaches (solid lines) with the best–guess estimate (dashed black line) according to Fig. 5. Please note that a data gap in the SOOP record was filled with two observations from SV *Tina V* (open circles in a).

https://doi.org/10.5194/bg-2021-40
Preprint. Discussion started: 1 March 2021

345 ± SD) across the observed productive period between July 6 and 24 was determined as 12.3 ± 2.5 m and 11.4 ± 2.3 m for the observational and model data, respectively (Fig. 6B). The TPD estimates are considerably higher than the respective mixed layer depth (MLD) estimates (6.0 ± 1.9 m and 5.5 ± 1.2 m) and agree better with the observed penetration depth of C_T* drawdown, indicating that TPD is the favourable approximation of the integration depth.

The NCP reconstruction based on TPD is generally higher than the MLD–based estimate (Fig. 6C). Comparing peak cumu-
350 lative NCP estimates for July 24, the TPD–approach results in a ~10% overestimation compared to the best–guess estimate, i.e. the value derived from vertically resolved measurements. In contrast, the MLD–based NCP estimate is ~30% lower than this best–guess estimate. The reconstructed NCP estimates are very similar for both test data sets, as the good agreement between the underlying C_T*, MLD and TPD time series suggests.

Comparing the deviation between the best–guess and reconstructed NCP estimates in the light of the lateral variability
355 observed within the study area, it must be emphasised that between July 6 and 24, the mean standard deviation of pCO_2 and C_T* across stations amounted to ± 6 μatm and ± 11 μmol kg^{-1}, respectively. This is higher than the likely uncertainty associated with the pCO_2 measurements (see Methods), as well as its response time correction (see Methods and Appendix A4) or conversion to C_T* (see Appendix C1). Therefore, the lateral variability of seawater chemistry and the production signal are generally considered the highest source of uncertainty to our NCP estimates. Still, this lateral variability is small compared
360 to the signal to be resolved (i.e. the C_T* consumption of ~90 μmol kg^{-1}), but on a relative scale (~10%) in about the same order of magnitude as the difference between the best–guess and the TPD–based, reconstructed NCP estimates. In contrast, the lateral variability is smaller than the deviation between the best–guess and the MLD–based, reconstructed NCP estimates.

All reconstructed NCP estimates include the correction of air–sea fluxes of CO_2, but it is impossible to quantify and correct vertical entrainment fluxes due to mixing, because the vertical distribution of C_T* across the water column can not be resolved.
365 The strong deviation between the best–guess NCP and the MLD-based reconstruction on August 16 is due to this missing correction of vertical mixing. This deviation highlights that the reconstruction approach is only applicable to production periods with a stable or shoaling thermocline. The TPD-based approach does not allow for any estimate during the last two weeks of the observations period, as the TPD is per definition only applicable to periods of warming surface waters.

4 Discussion

370 ### 4.1 Comparison to previous studies

Having in mind the application of our NCP reconstruction approach to other surface pCO_2 observation, it is important to examine if the biogeochemical dynamics of the 2018 cyanobacteria bloom investigated in this study is representative for those in other years. Unfortunately, only a few previous studies aimed at the quantification of cyanobacteria growth as a component of the Baltic Sea carbon budget. One exception is the interpretation of SOOP *Finnmaid* data by Schneider et al. (2014). Focusing
375 on the period from June to August and taking into consideration individual production pulses observed in the years 2005, 2008, 2009 and 2011, the authors found average daily rates of C_T* consumption ranging from 3 to 8 μmol kg^{-1} d^{-1}, which is comparable to the mean rate of 4.4 μmol kg^{-1} d^{-1} determined in this study (i.e. the average C_T* drawdown of ~90 μmol kg^{-1}

https://doi.org/10.5194/bg-2021-40
Preprint. Discussion started: 1 March 2021

over 12 days, Fig. 4). The individual production events identified by Schneider et al. (2014) lasted 1 to 5 weeks, similar to the duration described in this study. Finally, Schneider et al. (2014) also provided a depth–integrated NCP estimate based on a daily modelled mixing depths, which ranged from 3 – 20 m and were derived from the vertical distribution of a tracer one day after its injection into the surface. Although this approach is primarily useful to estimate the vertical distribution of air–sea CO_2 fluxes and does not necessarily reflect the vertical extent of net community production, their determined midsummer NCP estimates (1 – 2.1 mol m^{-2}) are in the same order of magnitude as the best–guess estimate derived in this study. It should be noted that the NCP estimates by Schneider et al. (2014) refer to the cumulative NCP of one to three production pulses per years, whereas our estimate of ~1.2 mol m^{-2} refers to a single bloom event.

Wasmund et al. (2001) conducted ^{14}C incubation experiments at different water depths to determine instantaneous rates of primary production during a cyanobacteria bloom. The obtained daytime carbon fixation rates in surface waters (0.4 – 0.8 mmol C m^{-3} h^{-1}) are in the same order of magnitude as the mean rate found in this study. More importantly, the authors also found significantly lower fixation rates below 10 m water depth (< 0.2 mmol–C m^{-3} h^{-1}), which agrees with the depth distribution of NCP observed in this study.

Furthermore, the succession of different cyanobacteria genera observed in 2018, with the *Nodularia* dominated bloom following an earlier presence of *Aphanizomenon* (Fig. B2), was previously described as a typical pattern (Wasmund, 2017), as well as the fact that increased wind speed and turbulence can inhibit N–fixation of cyanobacteria and cause the termination of the bloom (Wasmund, 1997).

In conclusion, the bloom event duration, C_T* drawdown, and NCP, as well as the vertical extend of carbon fixation and the succession of the bloom observed in this study agree well with observations in previous years, and distinct differences cannot be found. We therefore conclude that the findings of this study are representative for Baltic Sea cyanobacteria blooms in general, although the SST and pCO_2 levels in 2018 were at the upper and lower end, respectively, of the conditions observed in previous years (Schneider and Müller, 2018).

4.2 Recommendations and caveats for NCP reconstruction from SOOP and model data

The good agreement between our best–guess and the reconstructed, TPD-based NCP estimate of the production peak on July 24 (Fig. 6C) indicates that it is possible to determine NCP from surface pCO_2 observations and vertically resolved seawater temperature with little uncertainty. For the NCP calculation based on surface pCO_2 observations from SOOP and modelled temperature profiles, we recommend to:

1. Convert surface pCO_2 to C_T* based on a mean A_T estimate for the region under consideration.
2. Identify production pulses dominated by cyanobacteria as periods characterised by a decrease in C_T* that occurs between June and August.
3. Integrate observed surface C_T* changes to the temperature penetration depth (TPD) estimated from modelled temperature profiles, rather than using a mixed layer depth (MLD) estimate.

https://doi.org/10.5194/bg-2021-40
Preprint. Discussion started: 1 March 2021

4. Perform the integration individually for each production pulse and limit NCP reconstruction to periods characterised by a stable or shoaling thermocline.

It should be emphasised that lateral variability and water mass transport are critical for observation–based NCP estimates and constitute the largest source of uncertainty in our estimates. However, SOOP observations allow averaging of observations across large regions, which reduces the impact of lateral water mass transport (Schneider and Müller, 2018). The region for spatial averaging should be chosen large enough to avoid as much as possible the influence of lateral perturbations which depend on the surface dynamics and the biogeochemical gradients in the surrounding area. Yet, the region for spatial averaging should be chosen small enough to ensure that variations of $p\mathrm{CO}_2$ within the region are small compared to the temporal changes of interest. Another critical aspect of the recommended NCP reconstruction approach is the restriction to periods of a stable or shoaling thermocline. While in principle it is possible that net organic matter production could occur also during periods of a deepening thermocline, this process was observed neither in this study nor previous years (Schneider and Müller, 2018), and is in line with the planktological finding that increased wind speed causes the termination of the bloom (Wasmund, 1997).

The NCP reconstruction approach presented in this study was derived from observations covering a single bloom event within the Central Baltic Sea. In the lack of comparable comprehensive observational data that underlie our best–guess estimate, the applicability of this approach could not be tested for other regions or bloom events. However, the dynamics and intensity of the bloom event described here are comparable to previous, independent descriptions of cyanobacteria blooms. Therefore, it is assumed that underlying biogeochemical mechanisms are representative and that the NCP reconstruction approach can be applied to other cyanobacteria bloom events. Specifically, we assume that the findings represented here can be applied to evaluate past and future $p\mathrm{CO}_2$ observations made on *Finnmaid* and other SOOP in the Central Baltic Sea without compromise. Larger uncertainties should be expected when applying the approach to other basins of (or even outside) the Baltic Sea.

5 Conclusions

In this study, the depth–integrated quantification of NCP that occurred during a cyanobacteria bloom in the Baltic Sea in 2018 is achieved through the interpretation of profiling measurements of $p\mathrm{CO}_2$ that covered the entire bloom event. Furthermore, it is demonstrated that this best–guess estimate can be reconstructed with small bias from SOOP $p\mathrm{CO}_2$ observations and modelled temperature profiles. Recommendations to apply our reconstruction approach to the comprehensive long-term record of surface $p\mathrm{CO}_2$ data available for the Baltic Sea are given. The application of this approach will allow for the detection and attribution of trends in cyanobacteria NCP across decades. In particular the comparison of NCP estimates of bloom events that occurred under different environmental conditions will provide a better understanding of the controlling factors. Ultimately, this knowledge will inform the design and monitoring of conservation measures aiming at a Good Environmental Status of the Baltic Sea and potentially other regions.

https://doi.org/10.5194/bg-2021-40
Preprint. Discussion started: 1 March 2021

Code and data availability.

Website: Following the concept of literature programming and relying on the R package workflowr (Blischak et al., 2019), the code, plain text comments, and graphical output of this study are compiled as a website available at: https://jens-daniel-mueller.github.io/BloomSail/.

Code and raw data: A release of the Github repository underlying the website and containing all code was tagged as "os-2020-120_submission" and archived on https://zenodo.org/. All raw data required to run the analysis were uploaded manually to this archive. Thus, the combined code and data are available under doi: https://doi.org/10.5281/zenodo.4553314.

Processed environmental data: Processed in situ observation of this study will be made available through https://www.pangaea.de/ upon acceptance of the manuscript.

https://doi.org/10.5194/bg-2021-40
Preprint. Discussion started: 1 March 2021


Biogeosciences Discussions

Appendix A: pCO_2 sensor measurements

A1 Sensor calibration

The CONTROS HydroC® CO_2 sensor used in this study (serial number CO_2-0618-001) was calibrated in water by the manufacturer at 15 °C before (June 2018) and after (October 2018) the deployment for a measuring range of 100 to 500 μatm. The pre– and post–deployment calibration polynomials met the 6 steps per calibration with an R^2 of 0.999999 (pre) and 0.999993 (post) at an RMSE of 0.13 μatm (pre) and 0.43 μatm (post). The time between the calibrations was about 107 days and the sensor runtime during this interval was about 506 hours or little more than 21 days. The zero drift observed between the two calibrations was only 0.89 μatm.

A2 Sensor configuration and operation

The instrument periodically records zeroing values, during which the CO_2 within the gas stream is scrubbed by a soda lime cartridge. Zeroings of two minutes duration were recorded every five hours during the field deployment. A period of 600 seconds after the zeroing was flagged as a flush period, during which the sensor signal recovers to environmental conditions. Recordings during the flush and zeroing period were removed before further biogeochemical interpretation.

For the majority of the measurements, the sensor was operated with a 8W–pump (SBE-5T; Sea-Bird Electronics, Bellevue, USA) and the logging interval was set to 1 second. Only for the first two cruise days on July 6 and 10, a 1W–pump (SBE-5M, Sea-Bird Electronics) was used and the logging interval set to 10 seconds.

The downcast profiles were always recorded continuously and with a steady profiling speed of ~2 m min^{-1}. The upcast profiles were either performed continuously as well, or with a stop to record an equilibrated reference pCO_2 value at a desired depth. Only continuous downcast profiles were used for biogeochemical interpretation.

Zeroing signals were recorded by the CTD unit from the analogue sensor output, as well as in the internal sensor memory. Both records were used to ensure exact temporal match of the CTD and pCO_2 time series. Only pCO_2 data stored with higher temporal resolution in the internal memory were used during further analysis.

A3 Data post–processing

A drift correction as discussed in Fietzek et al. (2014) was applied to the field data to improve the data quality. This post–processing considers information from the pre– and post–deployment calibrations (i.e. concentration dependent or span drift) and the regular in situ zeroings (i.e. zero drift).

The first 60 seconds within every zeroing interval were discarded to only consider smooth zero–gas measurements that are not affected by the signal drop from ambient pCO_2 to the zero value. Zero signals for every point of the deployment were obtained by linear interpolation of the zero measurements. In case of data gaps larger than 2 hours within the deployment data, the course of the 2 zero signals before or after the gap was linearly extrapolated forward or backward, respectively, instead of an interpolation over the time of the measuring gap. A concentration–dependent drift of the sensor was considered

https://doi.org/10.5194/bg-2021-40
Preprint. Discussion started: 1 March 2021

by transforming the pre– into the post–deployment calibration polynomial according to the actual sensor runtime (and not according to the course of the zero measurements as applied within Fietzek et al. (2014)).

Approx. 100 unrealistic outliers were found within the sensor temperature record (T_{sensor} parameter) of the HydroC®. These were identified to be electronic artefacts and the values replaced by the constant temperatures recorded before and after these events that only lasted a few seconds at most.

Given the statistics of the pre– and post–deployment calibration, the small drift encountered throughout the deployment and the otherwise smooth performance of the sensor during the deployment, the accuracy of the measurements is considered to be 1% of reading as also found within Fietzek et al. (2014).

A4 pCO_2 response time correction

The actual in situ response times (τ) of the sensor were determined by fitting an exponential function to the signal recovery following a zeroing (Fig A1; Fiedler et al. (2013); Fietzek et al. (2014)). The determined τ values were used subsequently to correct the signal delay (Fiedler et al., 2013; Fietzek et al., 2014; Atamanchuk et al., 2015).

A4.1 Response time determination

In situ response times (τ) were determined from pCO_2 data recorded during the flush period after each zeroing. Data recorded during the initial 20 seconds of each flush period were removed as those are affected by the mixing of residual gas volumes inside the sensor. Individual τ values were determined by fitting the non–linear model

$$pCO_2(t) = pCO_2(t_{end}) + (pCO_2(t_0) - pCO_2(t_{end})) \cdot e^{(-dt/\tau)} \tag{A1}$$

where $pCO_2(t)$ is the recorded pCO_2 at time t, $pCO_2(t_0)$ and $pCO_2(t_{end})$ are the fitted pCO_2 values at the beginning and the end of the equilibration process, and *dt* is the time since the beginning of the equilibration process. In situ τ was determined for a fit interval length of 300 seconds. Flush periods were discarded when the mean of absolute residuals from the fit exceeded 1% of the final pCO_2, a condition which indicated unstable environmental pCO_2 (e.g. due to unintended heaving of the sensor package).

Similar to previous studies, a decrease of τ with increasing in situ temperature was found. The dependence of τ on temperature was fitted with linear regression models, separately for the deployments with the 1W– and 8W–pump. The sensor was carefully cleaned after each cruise and no signs of a changing sensor response time over time as an indicative of fouling on the sensor's membrane were detected.

A4.2 Correction procedure

For each recorded pCO_2 value, the corresponding τ was calculated from measured in situ temperature. The response time correction was then applied according to equation (S3) in the supplementary material of Bittig et al. (2018):

$$pCO_{2,insitu} = \frac{1}{2b} \cdot (pCO_{2,obs}(t_{i+1}) - a \cdot pCO_{2,obs}(t_i)); \qquad a = 1 - 2b, \qquad b = \left(1 + 2\frac{\tau}{t_{i+1} - t_i}\right)^{-1} \tag{A2}$$

https://doi.org/10.5194/bg-2021-40
Preprint. Discussion started: 1 March 2021

Biogeosciences Discussions Open Access EGU

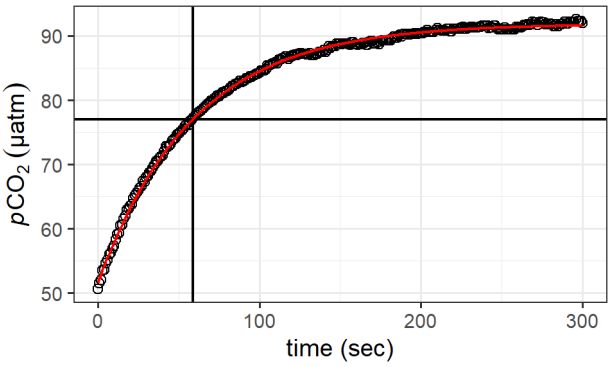

Figure A1. Exemplary determination of the response time τ through fitting an exponential function (red curve) to the $p\mathrm{CO}_2$ signal recovery following a zeroing measurement. The determined response time τ and $p\mathrm{CO}_2$(t=τ) are indicated by a vertical and horizontal line, respectively.

where $p\mathrm{CO}_{2,insitu}$ is the true in situ $p\mathrm{CO}_2$ time series, $p\mathrm{CO}_{2,obs}$ the $p\mathrm{CO}_2$ time series as recorded by the sensor, and τ the response time for the interval between t_i and t_{i+1}. Due to the short interval between adjacent observations in our study, the calculated value from the right side of equation A2 was considered directly representative for $p\mathrm{CO}_{2,insitu}(t_{i+1})$, although it is strictly the mean value between two adjacent observations, i.e. $0.5 \cdot (p\mathrm{CO}_{2,insitu}(t_i) + p\mathrm{CO}_{2,insitu}(t_{i+1}))$. Finally, a rolling mean with a window width of 30 sec was applied to the response time corrected $p\mathrm{CO}_{2,insitu}$ time series to remove short term noise. Please note that throughout the rest of the manuscript $p\mathrm{CO}_{2,insitu}$ is referred to as $p\mathrm{CO}_2$.

A4.3 Quality assessment

The improvements by the response time correction were investigated based on the difference between up- and downcast $p\mathrm{CO}_2$ profiles vertically gridded into 1m depth intervals. To focus this quality assessment on the conditions in near surface waters which are subject of this study, profiles were discarded which exceeded a maximum depth of 30 m and/or a maximum $p\mathrm{CO}_2$ of 300 μatm. Those profiles were excluded only for the quality assessment (not for the biogeochemical interpretation) to avoid a bias through exposure to very high $p\mathrm{CO}_2$ at greater depth. Furthermore, profiles were removed with a maximum number of missing observations from two or more depth intervals, which occasionally occurred when a sensor zeroing started while profiling. Based on this subset of response time corrected $p\mathrm{CO}_2$ profiles it was found that the mean absolute $p\mathrm{CO}_2$ difference between the up– and downcast profile was <2.5 μatm averaged across the upper 5 m of the water column and <7.5 μatm across the upper 20 m. The highest offset was found at around 10 m water depth and results from the steep environmental $p\mathrm{CO}_2$ gradient around the thermocline.

https://doi.org/10.5194/bg-2021-40
Preprint. Discussion started: 1 March 2021

Biogeosciences
Discussions
Open Access
EGU

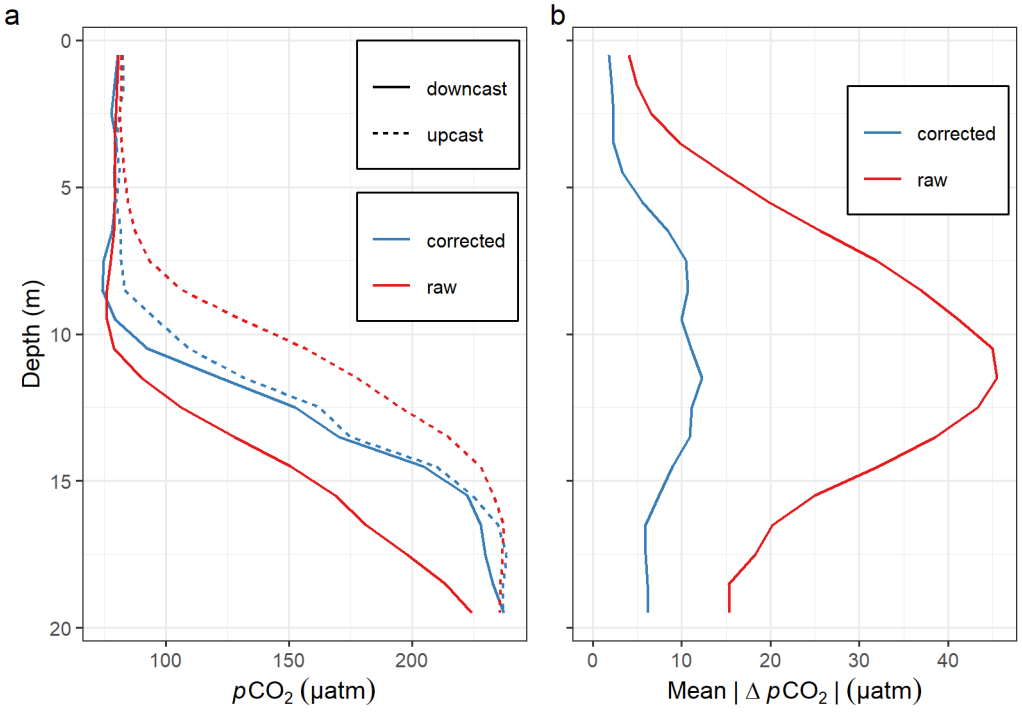

Figure A2. Comparison of pCO_2 profiles before (raw) and after (corrected) response time correction: (a) Exemplary up– and downcast pCO_2 profiles at one station and (b) mean absolute pCO_2 difference between up– and downcast profiles across all profiles included in the quality assessment.

https://doi.org/10.5194/bg-2021-40
Preprint. Discussion started: 1 March 2021

Appendix B: Discrete samples

B1 C_T and A_T

Dissolved inorganic carbon (C_T) was determined from discrete bottle samples with an Automated Infra Red Inorganic Carbon Analyzer (AIRICA, MARIANDA, Kiel, Germany). The analysis relies on the stripping of CO_2 through acidification. The released CO_2 is transported with a nitrogen carrier gas stream to an infrared detection unit (LI-7000, LI-COR Biosciences, Lincoln, USA), where the peak area is determined. Comparison to measurements performed on certified reference materials (CRM Batch 173; Dickson et al., 2003) allows for the calculation of C_T. Triplicated measurements were performed on each sample and a precision of 2 μmol kg^{-1} was achieved.

Total alkalinity (A_T) was analysed by open cell titration of 125 – 140 g of sample. The method involves a two–stage titration. After a first, single addition of hydrochloric acid to achieve a pH 4 – 3.5, A_T is determined during a continued, stepwise titration to pH 3, during which pH is recorded potentiometrically (Dickson et al., 2007). Measurements were referenced to CRM batch 173 (Dickson et al., 2003).

C_T* calculated for discrete samples refers to a classical alkalinity–normalised C_T, and was defined as $C_T^* = C_T \cdot A_{T,mean} / A_T$. C_T* derived from discrete samples or pCO_2 sensor data are directly comparable (Fig. 5c) because they are referenced to the same mean A_T of the discrete samples (1720 μmol kg^{-1}).

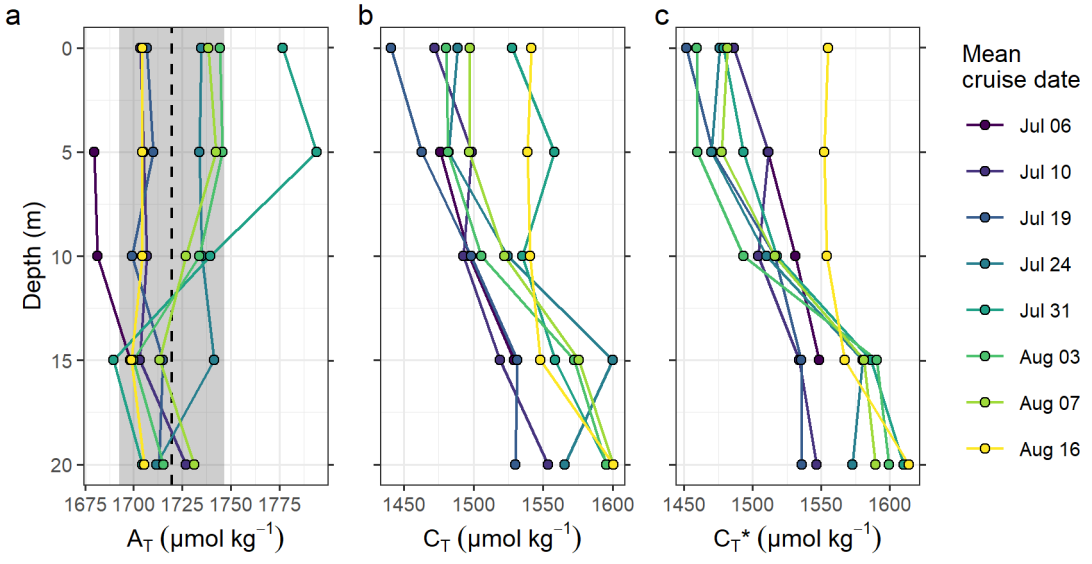

Figure B1. Vertical profiles of (a) A_T, (b) C_T, and (c) C_T normalised to the mean alkalinity (C_T*). Shown are cruise mean values for discrete samples taken at stations 07 and 10. The dashed line and grey area in (a) indicate the mean ± 1 standard deviation of A_T across the upper 20 m of the water column.

https://doi.org/10.5194/bg-2021-40
Preprint. Discussion started: 1 March 2021

B2 Phytoplankton

Phytoplankton samples were fixed with Lugol solution within no more than 24 hours after sampling. Samples were stored dark, before being transported to IOW and analysed in the laboratory within no more than 3 months after sampling. Phytoplankton community composition and biomass were determined by the Utermöhl method (HELCOM, 2017), which relies on microscope counts and the conversion of cell shape and size to biomass units.

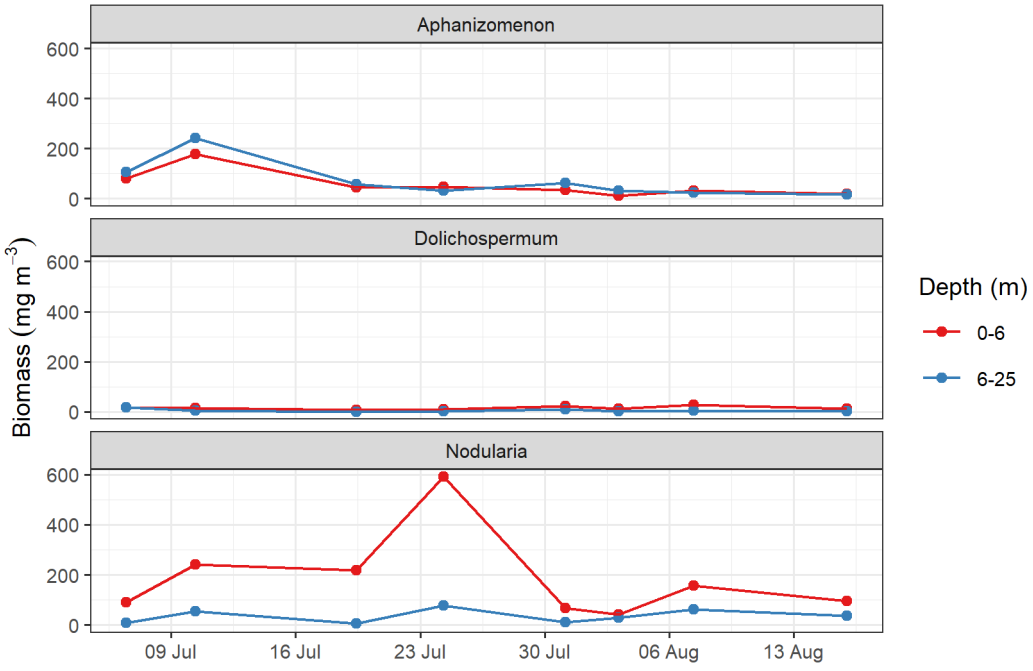

Figure B2. Time series of cyanobacterial biomass, averaged for surface (0 – 6 m) and subsurface (6 – 25 m) water masses sampled from stations 07 and 10 (Fig. 1). Results are based on microscope counts and distinguish three genera (panels).

https://doi.org/10.5194/bg-2021-40
Preprint. Discussion started: 1 March 2021

Appendix C: Net community production estimation

C1 Conversion from pCO_2 to C_T*

The approach to estimate temporal changes (rather than absolute values) in the dissolved inorganic carbon concentration (C_T) from a pCO_2 time series was previously established and theoretically examined (Schneider et al., 2014, and references therein). It relies on a fixed estimate of alkalinity (A_T) and is only applicable when noticeable internal changes in A_T can be excluded, as is the case in the Baltic Sea due to the absence of calcifying plankton (Tyrrell et al., 2008). To avoid confusion with measured or absolute C_T values and for consistency with previous studies, the calculated variable is referred to as C_T*.

To evaluate the applicability of this approach under the specific pCO_2 and temperature conditions observed in summer 2018, we calculated C_T* changes between Jul 6 and 24 for a range of A_T values covering three times the standard deviation of A_T observations (Fig. B1). For assumed A_T values of 1747 μmol kg^{-1} and 1693 μmol kg^{-1}, which is 1 standard deviation of the observations (27 μmol kg^{-1}) higher and lower than the mean A_T (1720 μmol kg^{-1}), the bias of the derived change in C_T* amounts to $\pm$ 1.6 μmol kg^{-1}. This bias is <2% compared to the signal of interest, i.e. the absolute drawdown of C_T* (89 μmol kg^{-1}).

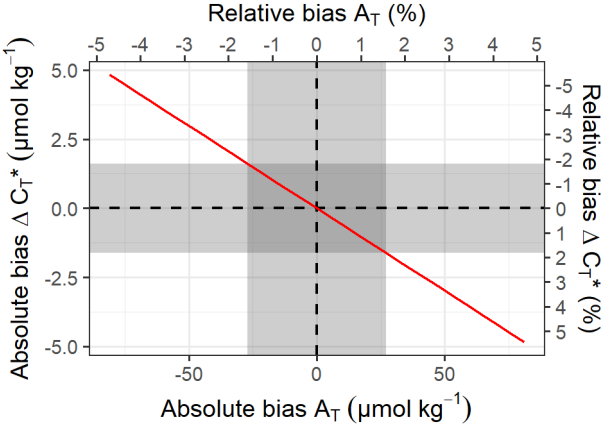

Figure C1. Bias of changes in C_T* as a function of the bias in mean A_T used for calculation (see Fig. B1). Results correspond to the pCO_2 and temperature conditions observed in this study and are expressed in absolute and relative units. Grey areas highlight $\pm$1 standard deviation around the mean A_T.

It should be noted that the bias assessment presented here reflects two types of errors, namely (i) the assignment of an erroneous mean A_T value for the calculation and (ii) the lateral exchange of water masses with different A_T but identical initial pCO_2 during the observation period. The robustness of this approach to the latter aspect is the reason why pCO_2 observations are more suitable to determine NCP than direct C_T measurements, when those are not normalised to corresponding A_T measurements.

https://doi.org/10.5194/bg-2021-40
Preprint. Discussion started: 1 March 2021

C2 Calculation of the vertical entrainment flux of C_T*

565 The vertical entrainment flux of C_T* that occured across the 12 m integration depth layer between Aug 7 and 16 was estimated assuming an instantaneous complete vertical mixing to 17 m water depth after Aug 7. For this scenario, the hypothetical homogeneous C_T* concentration after the mixing event (C_T*mix) equals the mean volume–weighted C_T* concentration between 0 – 17 m (Fig. C2). Furthermore, the entrainment flux (C_T*flux) into the surface water column (0 – 12 m) is equal to the concentration difference between observed C_T* on Aug 7 and C_T*mix, integrated from 12 to 17 m.

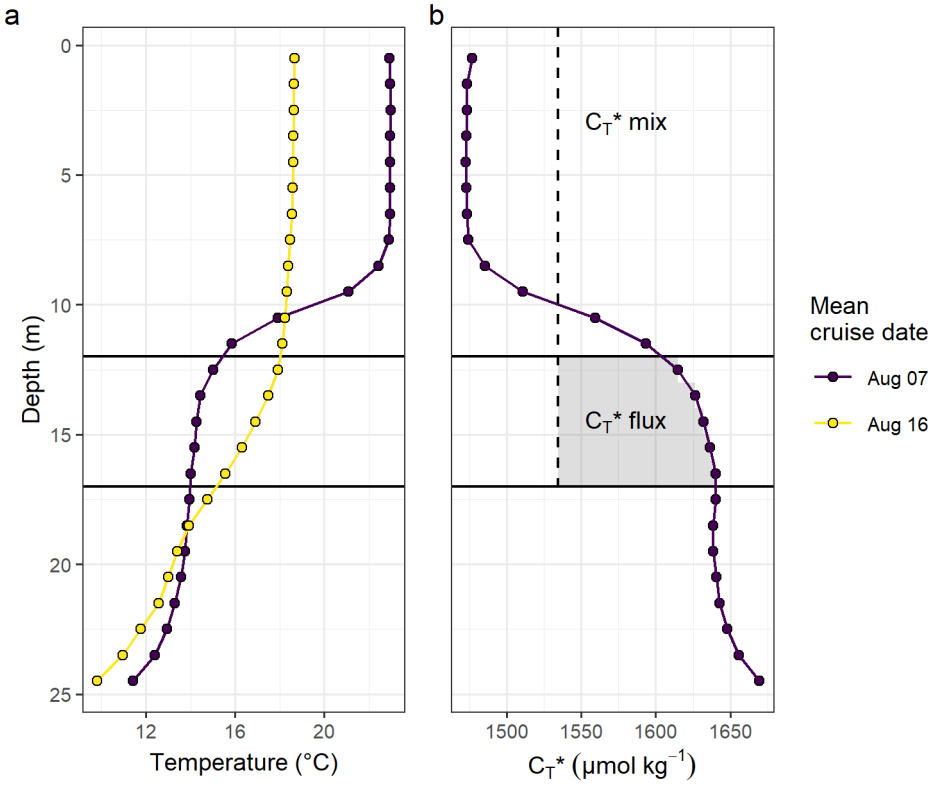

Figure C2. Illustration of the approximation of the entrainment flux of C_T* due to vertical mixing. (a) The estimated deepening of the mixed layer from 12 to 17 m water depth between Aug 7 and 16 is based on the observed changes in the temperature profiles. (b) Assuming a complete, instantaneous mixing of the water column after Aug 7, the hypothetical homogeneous concentration of C_T* (C_T*mix) can be used to approximate the entrainment flux of C_T* (grey area).

https://doi.org/10.5194/bg-2021-40
Preprint. Discussion started: 1 March 2021

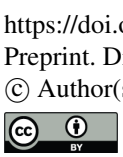

Biogeosciences
Discussions
Open Access
EGU

570 **C3 Individual stations profiles**

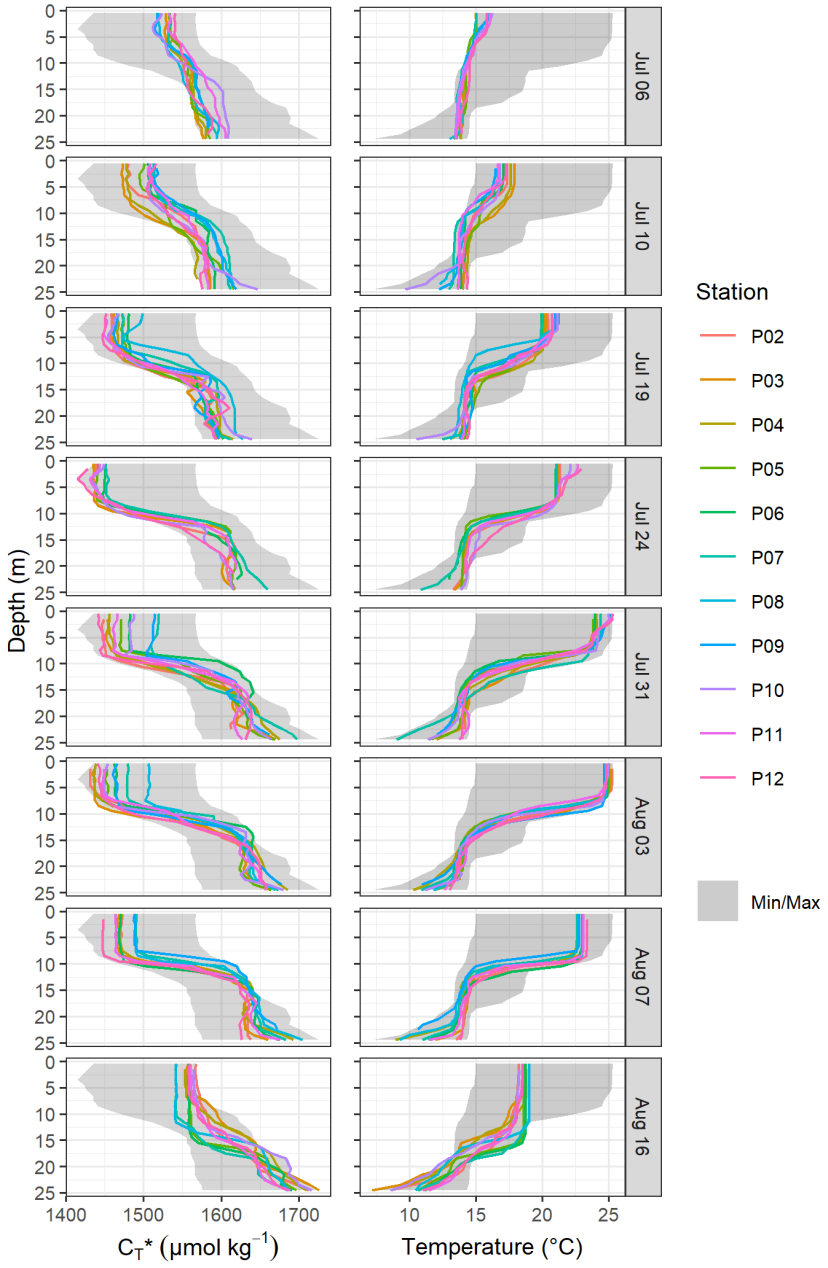

Figure C3. Individual profiles of C_T* (left panels) and temperature (right) displayed separately for each cruise day (rows) and station (color). Grey ribbons indicate the minimum and maximum values observed across the entire study period.

https://doi.org/10.5194/bg-2021-40
Preprint. Discussion started: 1 March 2021

C4 Temperature penetration depth (TPD) concept

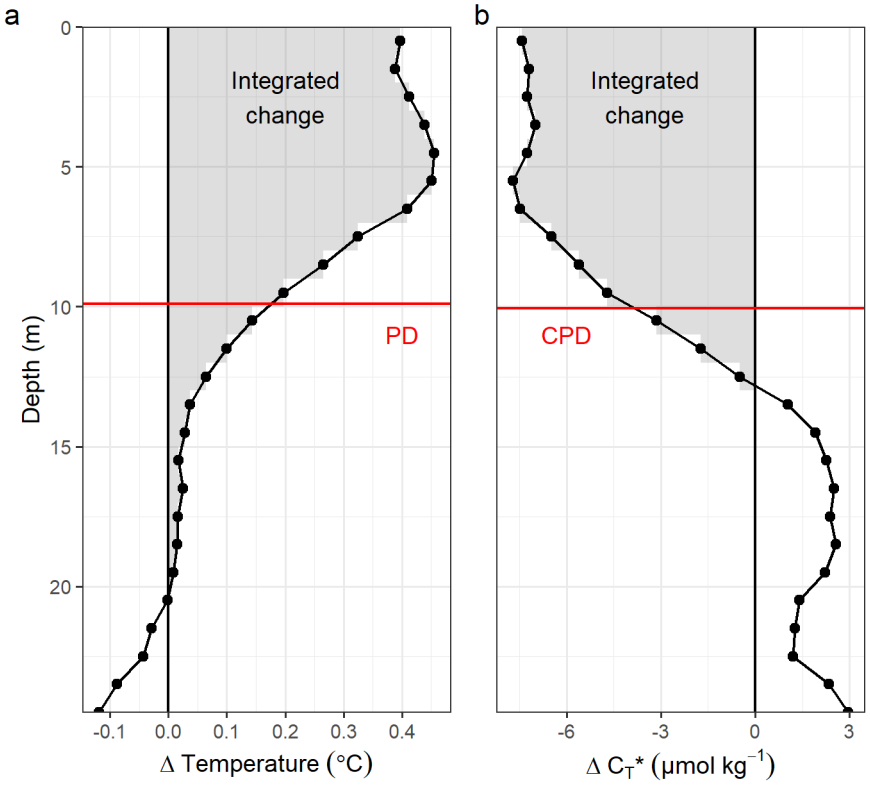

Figure C4. Illustration of the temperature and C_T* penetration depth concept, short TPD and CPD. Shown are exemplary profiles of incremental changes of (a) temperature and (b) C_T* observed between the cruises on July 6 and 10. TPD and CPD (red horizontal lines) are defined as the depth–integrated positive (for temperature) and negative (for C_T*) changes (grey areas) divided by the change at the surface. TPD and CPD are expressed in units of metres.

https://doi.org/10.5194/bg-2021-40
Preprint. Discussion started: 1 March 2021


Biogeosciences Discussions
Open Access
EGU

Appendix D: SOOP *Finnmaid* pCO_2

For SOOP *Finnmaid* transects recorded between July 7 and July 16, pCO_2 data were not available from the LI-COR system because of technical failure. Therefore, data generated by the Los Gatos (LGR) system were used to fill the gap. Unfortunately, the comparison of LI-COR and LGR measurements before July 7 indicated a small leakage in the LGR system, which was later also physically detected and fixed. The resulting difference between the two systems was clearly correlated with absolute pCO_2, as expected from contamination with ambient air. For data from the transect on July 5, the linear regression model $pCO_{2,true}$ = $pCO_{2,LGR}$ + 0.038 * $pCO_{2,LGR}$ - 24.2 was fitted, assuming that the LI-COR system had delivered the "true" $pCO_{2,true}$ before its failure. Assuming further that the effect of the contamination remained constant, this relationship was then applied to reconstruct $pCO_{2,true}$ from $pCO_{2,LGR}$ for the period without LI-COR data. To validate this adjustment, $pCO_{2,true}$ was also reconstructed from $pCO_{2,LGR}$ on July 4 and compared to pCO_2 directly measured with the LI-COR system. The mean difference was below 2 μatm for the entire transect as well as for a data subset within the study region, giving confidence to the high accuracy of the adjusted $pCO_{2,true}$. It should be noted that the adjusted SOOP pCO_2 data recorded between July 7 and July 16 agree well with the in situ pCO_2 recorded by the sailing campaign, i.e. the standard deviations of all surface measurements in the study region overlap.

https://doi.org/10.5194/bg-2021-40
Preprint. Discussion started: 1 March 2021

Author contributions. JDM was the lead author of this study and involved in all parts of it, in particular the conceptualization, funding acquisition, project administration, field sampling, data curation, visualisation and analysis, and manuscript writing. BS was involved in the conceptualization, formal analysis, and original draft preparation. UG generated and processed the GETM model data. PF supported the HydroC® sensor configuration and performed the data post processing. MBW and AR provided the atmospheric data and supported the field campaign logistically. NW was responsibly for the collection, analysis and interpretation of phytoplankton samples. SK designed and assembled the sensor package. GR was involved in the conceptualization, funding acquisition, and project administration and supervision. All authors contributed to the internal review and editing of the manuscript.

Competing interests. The authors declare that they have no conflict of interest.

Acknowledgements. The BloomSail expedition would not have been possible without the tremendous support of a fantastic group of people. In particular, 13 sailors supported the activities at sea. In the order of presence on board, those are Friederike Saathoff, Yannic Wocken, Andreas Kubatzki, Amanda Nylund, Rainer Kroiß, Ben Ole Grabler, Anna von Brandis, Fynn Pasewald, Ronja Topp, Matthias Kreuzburg, Katharina Klehmet, Mareike Körner, and Bastian Wulf. Monika Gerth supported the expedition by providing regular remote sensing products. Stefan Otto, Jenny Jeschek and Paul Cwierz supported the analysis of discrete samples. Furthermore, the authors are thankful for logistic and administrative support received from IOW (Beatrix Blabusch, Barbara Hentzsch, Kristin Beck) as well as in the harbour of Herrvik (Mats Hanson, Kenneth Broscheit). Technical equipment of the sailing vessel was supported among others by Segelwerkstatt Warnemünde, Lopolight, Delius Klasing, BMS, and Kadematic. We acknowledge the use of imagery from the NASA Worldview application (https://worldview.earthdata.nasa.gov/), part of the NASA Earth Observing System Data and Information System (EOSDIS). Furthermore, JDM acknowledges the funding of an early career grant received from the National Geographic Society through grant number EC-178R-18, as well as inhouse funding received from IOW. The research leading to this manuscript has received funding from BONUS, the joint Baltic Sea research and development programme (Art 185), funded jointly from the European Union's Seventh Programme for research, technological development and demonstration and from the German Federal Ministry of Education and Research through Grant No. Grant No. 03F0773A (BONUS INTEGRAL). Measurements on SOOP Finnmaid are a German contribution to the Integrated Carbon Observation System (ICOS), and received funding through the German Federal Ministry of Education and Research and the German Federal Ministry of Transport and Digital Infrastructure. The ICOS station Östergarnsholm is funded by the Swedish Research Council and Uppsala University.

https://doi.org/10.5194/bg-2021-40
Preprint. Discussion started: 1 March 2021

References

Atamanchuk, D., Tengberg, A., Aleynik, D., Fietzek, P., Shitashima, K., Lichtschlag, A., Hall, P. O. J., and Stahl, H.: Detection of CO2 leakage from a simulated sub-seabed storage site using three different types of pCO2 sensors, International Journal of Greenhouse Gas Control, 38, 121–134, https://doi.org/10.1016/j.ijggc.2014.10.021, 2015.

Axell, L. B.: Wind-driven internal waves and Langmuir circulations in a numerical ocean model of the southern Baltic Sea, J. Geophys. Res., 107, 3204, https://doi.org/10.1029/2001JC000922, 2002.

Bakker, D. C. E., Pfeil, B., Landa, C. S., Metzl, N., O'Brien, K. M., Olsen, A., Smith, K., Cosca, C., Harasawa, S., Jones, S. D., Nakaoka, S.-i., Nojiri, Y., Schuster, U., Steinhoff, T., Sweeney, C., Takahashi, T., Tilbrook, B., Wada, C., Wanninkhof, R., Alin, S. R., Balestrini, C. F., Barbero, L., Bates, N. R., Bianchi, A. A., Bonou, F., Boutin, J., Bozec, Y., Burger, E. F., Cai, W.-J., Castle, R. D., Chen, L., Chierici, M., Currie, K., Evans, W., Featherstone, C., Feely, R. A., Fransson, A., Goyet, C., Greenwood, N., Gregor, L., Hankin, S., Hardman-Mountford, N. J., Harlay, J., Hauck, J., Hoppema, M., Humphreys, M. P., Hunt, C. W., Huss, B., Ibánhez, J. S. P., Johannessen, T., Keeling, R., Kitidis, V., Körtzinger, A., Kozyr, A., Krasakopoulou, E., Kuwata, A., Landschützer, P., Lauvset, S. K., Lefèvre, N., Lo Monaco, C., Manke, A., Mathis, J. T., Merlivat, L., Millero, F. J., Monteiro, P. M. S., Munro, D. R., Murata, A., Newberger, T., Omar, A. M., Ono, T., Paterson, K., Pearce, D., Pierrot, D., Robbins, L. L., Saito, S., Salisbury, J., Schlitzer, R., Schneider, B., Schweitzer, R., Sieger, R., Skjelvan, I., Sullivan, K. F., Sutherland, S. C., Sutton, A. J., Tadokoro, K., Telszewski, M., Tuma, M., van Heuven, S. M. A. C., Vandemark, D., Ward, B., Watson, A. J., and Xu, S.: A multi-decade record of high-quality CO2 data in version 3 of the Surface Ocean CO2 Atlas (SOCAT), Earth System Science Data, 8, 383–413, https://doi.org/https://doi.org/10.5194/essd-8-383-2016, publisher: Copernicus GmbH, 2016.

Bittig, H. C., Körtzinger, A., Neill, C., van Ooijen, E., Plant, J. N., Hahn, J., Johnson, K. S., Yang, B., and Emerson, S. R.: Oxygen Optode Sensors: Principle, Characterization, Calibration, and Application in the Ocean, Front. Mar. Sci., 4, 429, https://doi.org/10.3389/fmars.2017.00429, 2018.

Blischak, J. D., Carbonetto, P., and Stephens, M.: Creating and sharing reproducible research code the workflowr way, F1000Res, 8, 1749, https://doi.org/10.12688/f1000research.20843.1, 2019.

Carstensen, J., Andersen, J. H., Gustafsson, B. G., and Conley, D. J.: Deoxygenation of the Baltic Sea during the last century, Proceedings of the National Academy of Sciences, 111, 5628–5633, https://doi.org/10.1073/pnas.1323156111, 2014.

Dickson, A. G., Afghan, J. D., and Anderson, G. C.: Reference materials for oceanic CO2 analysis: a method for the certification of total alkalinity, Marine Chemistry, 80, 185–197, https://doi.org/10.1016/S0304-4203(02)00133-0, 2003.

Dickson, A. G., Sabine, C. L., Christian, J. R., Bargeron, C. P., and Organization, N. P. M. S., eds.: Guide to best practices for ocean CO2 measurements, no. no. 3 in PICES special publication, North Pacific Marine Science Organization, Sidney, BC, oCLC: ocn420872251, 2007.

Fiedler, B., Fietzek, P., Vieira, N., Silva, P., Bittig, H. C., and Körtzinger, A.: In Situ CO2 and O2 Measurements on a Profiling Float, J. Atmos. Oceanic Technol., 30, 112–126, https://doi.org/10.1175/JTECH-D-12-00043.1, publisher: American Meteorological Society, 2013.

Fietzek, P., Fiedler, B., Steinhoff, T., and Körtzinger, A.: In situ Quality Assessment of a Novel Underwater pCO2 Sensor Based on Membrane Equilibration and NDIR Spectrometry, J. Atmos. Oceanic Technol., 31, 181–196, https://doi.org/10.1175/JTECH-D-13-00083.1, publisher: American Meteorological Society, 2014.

https://doi.org/10.5194/bg-2021-40
Preprint. Discussion started: 1 March 2021

Finni, T., Kononen, K., Olsonen, R., and Wallström, K.: The History of Cyanobacterial Blooms in the Baltic Sea, ambi, 30, 172–178, https://doi.org/10.1579/0044-7447-30.4.172, publisher: Royal Swedish Academy of Sciences, 2001.

Gattuso, J.-P., Epitalon, J.-M., Lavigne, H., and Orr, J.: seacarb: Seawater Carbonate Chemistry, https://CRAN.R-project.org/package=seacarb, 2020.

Gilly, W. F., Beman, J. M., Litvin, S. Y., and Robison, B. H.: Oceanographic and Biological Effects of Shoaling of the Oxygen Minimum Zone, Annual Review of Marine Science, 5, 393–420, https://doi.org/10.1146/annurev-marine-120710-100849, _eprint: https://doi.org/10.1146/annurev-marine-120710-100849, 2013.

Gräwe, U., Klingbeil, K., Kelln, J., and Dangendorf, S.: Decomposing Mean Sea Level Rise in a Semi-Enclosed Basin, the Baltic Sea, J. Climate, 32, 3089–3108, https://doi.org/10.1175/JCLI-D-18-0174.1, 2019.

Gülzow, W., Rehder, G., Schneider, B., Deimling, J. S. v., and Sadkowiak, B.: A new method for continuous measurement of methane and carbon dioxide in surface waters using off-axis integrated cavity output spectroscopy (ICOS): An example from the Baltic Sea, Limnology and Oceanography: Methods, 9, 176–184, https://doi.org/https://doi.org/10.4319/lom.2011.9.176, _eprint: https://aslopubs.onlinelibrary.wiley.com/doi/pdf/10.4319/lom.2011.9.176, 2011.

Hansell, D. A. and Carlson, C. A.: Net community production of dissolved organic carbon, Global Biogeochemical Cycles, 12, 443–453, https://doi.org/10.1029/98GB01928, _eprint: https://agupubs.onlinelibrary.wiley.com/doi/pdf/10.1029/98GB01928, 1998.

Hansson, M. and Hakansson, B.: The Baltic Algae Watch System - a remote sensing application for monitoring cyanobacterial blooms in the Baltic Sea, JARS, 1, 011 507, https://doi.org/10.1117/1.2834769, publisher: International Society for Optics and Photonics, 2007.

HELCOM: Guidelines for monitoring phytoplankton species composition abundance and biomass, https://www.helcom.fi/wp-content/uploads/2019/08/Guidelines-for-monitoring-phytoplankton-species-composition-abundance-and-biomass.pdf, 2017.

Henson, S. A., Sanders, R., Madsen, E., Morris, P. J., Moigne, F. L., and Quartly, G. D.: A reduced estimate of the strength of the ocean's biological carbon pump, Geophysical Research Letters, 38, https://doi.org/10.1029/2011GL046735, _eprint: https://agupubs.onlinelibrary.wiley.com/doi/pdf/10.1029/2011GL046735, 2011.

Kahru, M. and Elmgren, R.: Multidecadal time series of satellite-detected accumulations of cyanobacteria in the Baltic Sea, Biogeosciences, 11, 3619–3633, https://doi.org/10.5194/bg-11-3619-2014, 2014.

Kara, A. B., Hurlburt, H. E., and Wallcraft, A. J.: Stability-Dependent Exchange Coefficients for Air–Sea Fluxes, J. Atmos. Oceanic Technol., 22, 1080–1094, https://doi.org/10.1175/JTECH1747.1, 2005.

Karlson, A. M. L., Duberg, J., Motwani, N. H., Hogfors, H., Klawonn, I., Ploug, H., Barthel Svedén, J., Garbaras, A., Sundelin, B., Hajdu, S., Larsson, U., Elmgren, R., and Gorokhova, E.: Nitrogen fixation by cyanobacteria stimulates production in Baltic food webs, AMBIO, 44, 413–426, https://doi.org/10.1007/s13280-015-0660-x, 2015.

Kownacka, J., Busch, S., Göbel, J., Gromisz, S., Hällfors, H., Huseby, S., Jaanus, A., Jakobsen, H. H., Johansen, M., Johansson, M., Liebeke, N., Kraśniewski, W., Kremp, A., Lehtinen, S., Olenina, I., and Wasmund, N.: Cyanobacteria biomass, 1990-2019, https://helcom.fi/wp-content/uploads/2020/09/BSEFS-Cyanobacteria-biomass-1990-2019-1.pdf, 2020.

Kutser, T., Metsamaa, L., and Dekker, A. G.: Influence of the vertical distribution of cyanobacteria in the water column on the remote sensing signal, Estuarine, Coastal and Shelf Science, 78, 649–654, https://doi.org/10.1016/j.ecss.2008.02.024, 2008.

Löptien, U. and Meier, H. E. M.: The influence of increasing water turbidity on the sea surface temperature in the Baltic Sea: A model sensitivity study, Journal of Marine Systems, 88, 323–331, https://doi.org/10.1016/j.jmarsys.2011.06.001, 2011.

https://doi.org/10.5194/bg-2021-40
Preprint. Discussion started: 1 March 2021

Meier, H. E. M., Eilola, K., Almroth-Rosell, E., Schimanke, S., Kniebusch, M., Höglund, A., Pemberton, P., Liu, Y., Väli, G., and Saraiva, S.: Disentangling the impact of nutrient load and climate changes on Baltic Sea hypoxia and eutrophication since 1850, Clim Dyn, 53, 1145–1166, https://doi.org/10.1007/s00382-018-4296-y, 2019.

Millero, F. J.: Carbonate constants for estuarine waters, Mar. Freshwater Res., 61, 139, https://doi.org/10.1071/MF09254, 2010.

Mohrholz, V., Naumann, M., Nausch, G., Krüger, S., and Gräwe, U.: Fresh oxygen for the Baltic Sea — An exceptional saline inflow after a decade of stagnation, Journal of Marine Systems, 148, 152–166, https://doi.org/10.1016/j.jmarsys.2015.03.005, 2015.

Nausch, M., Nausch, G., Lass, H. U., Mohrholz, V., Nagel, K., Siegel, H., and Wasmund, N.: Phosphorus input by upwelling in the eastern Gotland Basin (Baltic Sea) in summer and its effects on filamentous cyanobacteria, Estuarine, Coastal and Shelf Science, 83, 434–442, https://doi.org/10.1016/j.ecss.2009.04.031, 2009.

Nausch, M., Nausch, G., Mohrholz, V., Siegel, H., and Wasmund, N.: Is growth of filamentous cyanobacteria supported by phosphate uptake below the thermocline?, Estuarine, Coastal and Shelf Science, 99, 50–60, https://doi.org/10.1016/j.ecss.2011.12.011, 2012.

Olofsson, M., Torstensson, A., Karlberg, M., Steinhoff, F. S., Dinasquet, J., Riemann, L., Chierici, M., and Wulff, A.: Limited response of a spring bloom community inoculated with filamentous cyanobacteria to elevated temperature and pCO2, Botanica Marina, 62, 3–16, https://doi.org/10.1515/bot-2018-0005, publisher: De Gruyter Section: Botanica Marina, 2019.

Olofsson, M., Suikkanen, S., Kobos, J., Wasmund, N., and Karlson, B.: Basin-specific changes in filamentous cyanobacteria community composition across four decades in the Baltic Sea, Harmful Algae, 91, 101 685, https://doi.org/10.1016/j.hal.2019.101685, 2020.

Oschlies, A., Brandt, P., Stramma, L., and Schmidtko, S.: Drivers and mechanisms of ocean deoxygenation, Nature Geoscience, 11, 467–473, https://doi.org/10.1038/s41561-018-0152-2, number: 7 Publisher: Nature Publishing Group, 2018.

Placke, M., Meier, H. E. M., Gräwe, U., Neumann, T., Frauen, C., and Liu, Y.: Long-Term Mean Circulation of the Baltic Sea as Represented by Various Ocean Circulation Models, Front. Mar. Sci., 5, 287, https://doi.org/10.3389/fmars.2018.00287, 2018.

Roquet, F., Madec, G., McDougall, T. J., and Barker, P. M.: Accurate polynomial expressions for the density and specific volume of seawater using the TEOS-10 standard, Ocean Modelling, 90, 29–43, https://doi.org/10.1016/j.ocemod.2015.04.002, 2015.

Rutgersson, A., Pettersson, H., Nilsson, E., Bergström, H., Wallin, M. B., Nilsson, E. D., Sahlée, E., Wu, L., and Mårtensson, E. M.: Using land-based stations for air–sea interaction studies, Tellus A: Dynamic Meteorology and Oceanography, 72, 1–23, https://doi.org/10.1080/16000870.2019.1697601, publisher: Taylor & Francis _eprint: https://doi.org/10.1080/16000870.2019.1697601, 2020.

Sanders, R., Henson, S. A., Koski, M., De La Rocha, C. L., Painter, S. C., Poulton, A. J., Riley, J., Salihoglu, B., Visser, A., Yool, A., Bellerby, R., and Martin, A. P.: The Biological Carbon Pump in the North Atlantic, Progress in Oceanography, 129, 200–218, https://doi.org/10.1016/j.pocean.2014.05.005, 2014.

Saraiva, S., Markus Meier, H. E., Andersson, H., Höglund, A., Dieterich, C., Gröger, M., Hordoir, R., and Eilola, K.: Baltic Sea ecosystem response to various nutrient load scenarios in present and future climates, Clim Dyn, 52, 3369–3387, https://doi.org/10.1007/s00382-018-4330-0, 2019.

Schneider, B. and Kuss, J.: Past and present productivity of the Baltic Sea as inferred from pCO2 data, Continental Shelf Research, 24, 1611–1622, https://doi.org/10.1016/j.csr.2004.06.023, 2004.

Schneider, B. and Müller, J. D.: Biogeochemical Transformations in the Baltic Sea, Springer Oceanography, Springer International Publishing, Cham, https://doi.org/10.1007/978-3-319-61699-5, 2018.

Schneider, B., Nausch, G., Nagel, K., and Wasmund, N.: The surface water CO2 budget for the Baltic Proper: a new way to determine nitrogen fixation, Journal of Marine Systems, 42, 53–64, https://doi.org/10.1016/S0924-7963(03)00064-2, 2003.

https://doi.org/10.5194/bg-2021-40
Preprint. Discussion started: 1 March 2021

Schneider, B., Kaitala, S., and Maunula, P.: Identification and quantification of plankton bloom events in the Baltic Sea by continuous pCO2 and chlorophyll a measurements on a cargo ship, Journal of Marine Systems, 59, 238–248, https://doi.org/10.1016/j.jmarsys.2005.11.003, 2006.

Schneider, B., Gustafsson, E., and Sadkowiak, B.: Control of the mid-summer net community production and nitrogen fixation in the central Baltic Sea: An approach based on pCO2 measurements on a cargo ship, Journal of Marine Systems, 136, 1–9, https://doi.org/10.1016/j.jmarsys.2014.03.007, 2014.

Tyrrell, T., Schneider, B., Charalampopoulou, A., and Riebesell, U.: Coccolithophores and calcite saturation state in the Baltic and Black Seas, Biogeosciences, p. 10, 2008.

Vahtera, E., Conley, D. J., Gustafsson, B. G., Kuosa, H., Pitkänen, H., Savchuk, O. P., Tamminen, T., Viitasalo, M., Voss, M., Wasmund, N., and Wulff, F.: Internal Ecosystem Feedbacks Enhance Nitrogen-fixing Cyanobacteria Blooms and Complicate Management in the Baltic Sea, ambi, 36, 186–194, https://doi.org/10.1579/0044-7447(2007)36[186:IEFENC]2.0.CO;2, publisher: Royal Swedish Academy of Sciences, 2007.

Wanninkhof, R.: Relationship between wind speed and gas exchange over the ocean revisited: Gas exchange and wind speed over the ocean, Limnol. Oceanogr. Methods, 12, 351–362, https://doi.org/10.4319/lom.2014.12.351, 2014.

Wasmund, N.: Occurrence of cyanobacterial blooms in the baltic sea in relation to environmental conditions, Internationale Revue der gesamten Hydrobiologie und Hydrographie, 82, 169–184, https://doi.org/https://doi.org/10.1002/iroh.19970820205, _eprint: https://onlinelibrary.wiley.com/doi/pdf/10.1002/iroh.19970820205, 1997.

Wasmund, N.: Recruitment of bloom-forming cyanobacteria from winter/spring populations in the Baltic Sea verified by a mesocosm approach, Boreal Env. Res., 22, 445–455, 2017.

Wasmund, N., Voss, M., and Lochte, K.: Evidence of nitrogen fixation by non-heterocystous cyanobacteria in the Baltic Sea and re-calculation of a budget of nitrogen fixation, Marine Ecology Progress Series, 214, 1–14, https://doi.org/10.3354/meps214001, 2001.

Wasmund, N., Nausch, G., Schneider, B., Nagel, K., and Voss, M.: Comparison of nitrogen fixation rates determined with different methods: a study in the Baltic Proper, Mar. Ecol. Prog. Ser., 297, 23–31, https://doi.org/10.3354/meps297023, 2005.

Winslow, L. A., Zwart, J. A., Batt, R. D., Dugan, H. A., Woolway, R. I., Corman, J. R., and Read, J. S.: LakeMetabolizer: An R package for estimating lake metabolism from free-water oxygen using diverse statistical models, 2016.

Zängl, G., Reinert, D., Rípodas, P., and Baldauf, M.: The ICON (ICOsahedral Non-hydrostatic) modelling framework of DWD and MPI-M: Description of the non-hydrostatic dynamical core, Q.J.R. Meteorol. Soc, 141, 563–579, https://doi.org/10.1002/qj.2378, 2015.